



A review on application of mechanical metamaterials for vibration control

Srajan Dalela, P. S. Balaji & D. P. Jena

To cite this article: Srajan Dalela, P. S. Balaji & D. P. Jena (2021): A review on application of mechanical metamaterials for vibration control, Mechanics of Advanced Materials and Structures, DOI: [10.1080/15376494.2021.1892244](https://doi.org/10.1080/15376494.2021.1892244)

To link to this article: <https://doi.org/10.1080/15376494.2021.1892244>



Published online: 26 Feb 2021.



Submit your article to this journal



Article views: 344



View related articles



View Crossmark data



ORIGINAL ARTICLE

A review on application of mechanical metamaterials for vibration control

Srajan Dalela^a, P. S. Balaji^a , and D. P. Jena^b

^aDepartment of Mechanical Engineering, National Institute of Technology, Rourkela, India; ^bDepartment of Industrial Design, National Institute of Technology, Rourkela, India

ABSTRACT

Mechanical metamaterials exhibit some superior mechanical properties such as ultrahigh strength-to-weight ratio, negative bulk-modulus, negative stiffness, negative mass-density, and negative Poisson's ratio. These advantages led to a variety of applications, especially in vibration isolation, by targeting and tuning for a specific frequency-range called stopband. The tuning ability is achieved from its array of unit-cells, which can be topologically optimized for the desired frequency range. This review discusses the development of mechanical metamaterials and focuses on its vibration control applications by using passive and active approaches for stopband enhancement and broadening the bandwidth at varying frequency-ranges.

ARTICLE HISTORY

Received 13 November 2019
Accepted 15 February 2021

KEYWORDS

Active; bandgap;
mechanical metamaterials;
passive; vibration control

1. Introduction

For the past few years, engineering material developments have entirely relied on modifying material properties by varying its composition. The materials are tailored with specific properties to meet the demand [1]. However, the development of materials with specific intrinsic properties is challenging since materials inherently possess definite intrinsic properties such as low strength materials to have low density and vice-versa [2]. Natural materials, particularly cellular materials, exhibit fascinating properties lacking in conventional materials by developing their optimized architecture [3]. A lot of efforts are made to reduce the coupling between the mass density and mechanical properties, and many topological designs have been proposed that reduce the size from macroscale to unit cell scale to give the same strength and properties. Recent developments in the Additive Manufacturing (AM) process, also known as 3D-Printing, enabled complex architecture modeling with length scale varying to nanometers for a different range of materials [4, 5]. The development in 3D printing resulted in further improvement in the mechanical properties of materials. The size of the material reduced to the nanoscale, which allows the strength to increase, also known as "smaller, is stronger." [6, 7]. The technical capability to build materials at very low scales (up to 10^{-9} m) leads to the development of newly devised materials known as "Metamaterials" whose acoustic and mechanical properties can be tailored as per the requirements [8, 9].

Metamaterials are artificially structured composites that are constructed using the periodically arranged building blocks, which not only enhance the properties of constituent materials but also give different functionalities and unusual

properties [10] like negative refractive index, negative mass density, negative Poisson's ratio, negative permittivity, negative permeability, negative bulk modulus, sign reversal of thermal expansion coefficient, etc. [11, 12]. Metamaterials have their properties altered to something beyond what is found in nature. Early metamaterials were introduced in the electromagnetic field for achieving negative permittivity and permeability for the experimental purpose [13], and later, the metamaterial concept was also extended to solid mechanics [14], elastic waves [15], acoustics [16, 17] and as a vibration absorber. A study on locally resonant phononic crystals leads to the starting of research on metamaterials [18] for vibration isolation purposes.

Mathematically arranging periodic structures on a continuum for getting effective and enhanced parameters is the main objective of homogenization theory [19, 20]. Nowadays, it is challenging to homogenize a periodic structure and map it into the required effective medium due to the continuous reduction in the cell's size from a micrometer to a nanometer. In this review, the architectures mentioned can get mapped onto effective parameters because the lattice constant taken is much smaller than the wavelength's characteristic length [21, 22]. Metamaterials can be classified based on the effective parameters, as shown in Figure 1. This review is mainly focused on wave attenuation using the physics of phononic crystals and local resonance for vibration control.

1.1. Mechanical metamaterials

Mechanical waves propagating through the acoustic metamaterial possess only longitudinally polarized waves, as the value of shear modulus G is zero in liquid and gas medium.

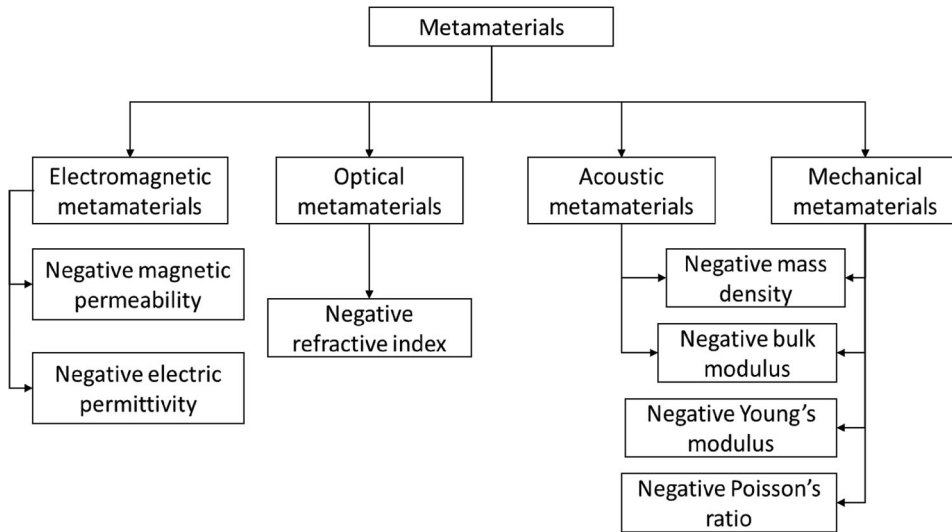


Figure 1. Classification of metamaterials.

To overcome this barrier, mechanical metamaterials were designed to study the effect of shear modulus on the mechanical waves. The crystalline elastic solid of mechanical metamaterials support both longitudinal and transverse waves, as these metamaterials exhibit all the four mechanical properties, i.e., elastic modulus/stiffness (E), bulk modulus (K), shear modulus (G), and Poisson's ratio (μ) [23].

In mechanical metamaterial, the unconventional desired properties are obtained by inducing negative effective material parameters [24]. The first experimental investigation for negative effective mass density was successfully defined using a silicon rubber-coated sphere embedded on epoxy [16]. Later, many studies were performed using nonlinear mass in mass system by defining negative effective mass density for vibration isolation, which gave good results [25]. Negative bulk modulus was experimentally proved at a resonant frequency in one-dimensional acoustic metamaterial using a subwavelength array of the Helmholtz resonators [26]. Thus by varying the shape, size, arrangement, and orientation of the micro-structure of constituent material, the mechanical metamaterial's exceptional properties can be derived. Figure 2 describes the formation of 3D material by using atoms to form the unit cell for crystalline solid (a, b) and then arranging unit cells in a continuous medium to form a crystalline structure (c). A specially designed unit cell is considered (d), it is arranged periodically or non-periodically as required (e) and then arranging them accordingly to get desired negative effective properties known as 3D metamaterial (f) [27].

The building block of mechanical metamaterial is meta-atom, which deform, buckle, rotate, snap under external forces; these meta-atoms then combine and design to yield the desired behavior. The basic building block of mechanical metamaterials is shown in Figure 3. The first part shows the slender elements, sharp tips, and creases. The bending stiffness of these elements varies with cubic power of thickness, so there is a localized bending in all three slender elements [29]. Bending increases with the increase in

angle, as shown in Figure 3(a). The second part (Figure 3b) shows the elastic beam inducing buckling property under axial compressive force, further recover their original shape after the unloading and also provide nonlinear but reversible meta-atoms for the metamaterial. The third part shows the constrained beam inducing the snap-through nature of the beam under buckling; this snap-through nature depends on the geometry and boundary conditions [30], as shown in Figure 3(c) [28].

The classification of mechanical metamaterials needs to be studied to understand the fascinating properties obtained from its exceptional behavior. They can be classified based on the mechanical properties, i.e., elastic modulus, bulk modulus, shear modulus, and Poisson's ratio.

Due to the boom in additive manufacturing techniques in recent years, there is a considerable increase in the number of methods to print high quality 3D cellular structures with complex architecture and in a wide range of sizes [31]. The successful application of mechanical metamaterial in nano/micro lattices has mostly been attributed to its capability to utilize complex architecture in recent years. The size effects in materials have also been reduced to the nanoscale, which allows the unconventional properties to be discovered.

This review is mainly focused on vibration control in varying frequency ranges using mechanical metamaterials in different ways. Section 1 introduced metamaterials. In Sect. 2, the basics of vibration and how it can be controlled is discussed. Section 3 discusses the bandgap mechanism of the metamaterials. Followingly, two different techniques for vibration control using mechanical metamaterial are discussed, such as—Passive metamaterial in Sect. 4, Active metamaterial in Sect. 5. There is a vast amount of literature on metamaterials; however, the prime focus is on the mechanical metamaterial for vibration control applications. The relevant and recent research are discussed, and within the capacity of the authors, this review provides comprehensive applications of metamaterial for vibration control. Finally,

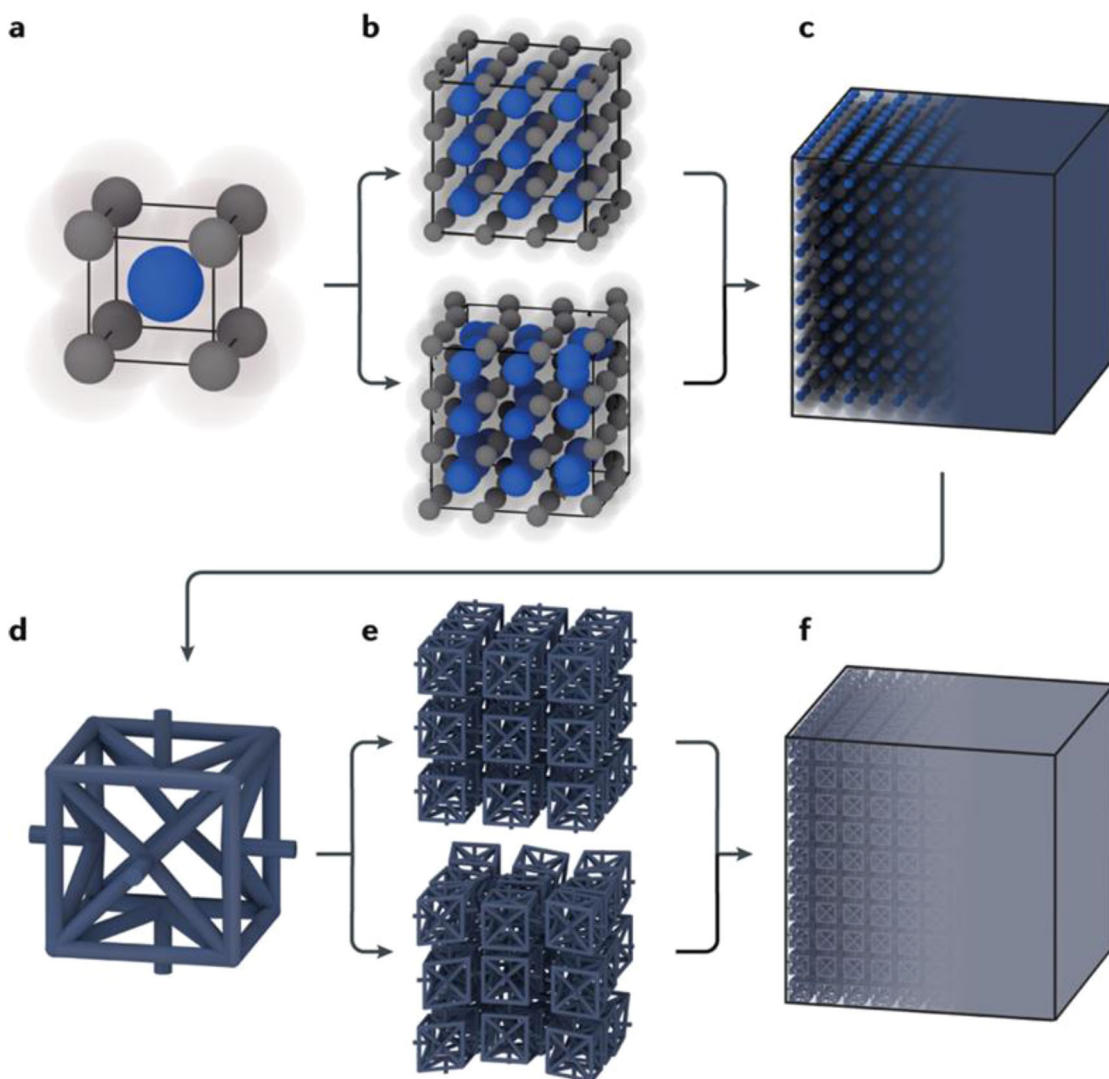


Figure 2. (a) Unit cell. (b) Unit cell for crystalline solid. (c) Crystalline structure. (d) A specially designed unit cell. (e) Unit cell for the 3D structure. (f) Structure of 3D metamaterial [27].

the review ends with discussing future research directions based on the detailed literature review performed.

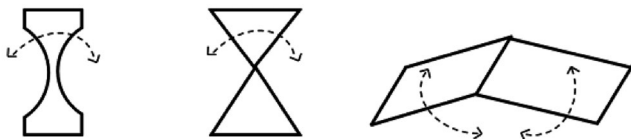
2. Vibration and its control

Vibration is a significant cause of concern as they cause fatigue and subsequent failures of the machines and structures that can result in numerous disasters, system performance degradation, human discomfort, and catastrophic failures. Examples of such vibration include vibrations from the operations of heavy machinery industries, vibrations in bridges due to vehicles, wind-induced vibrations of tall structures, etc. The adverse vibrational effects have motivated scientists and engineers to develop various materials, systems, and strategies to mitigate, suppress, or absorb these unwanted vibrations [32]. The undesirable effects of the disturbance transmitted to the receiver from the source can be reduced by providing a wave barrier in the transmission path. The wave barrier disrupts the vibration path from the source to the receiver [33, 34], as shown in Figure 4.

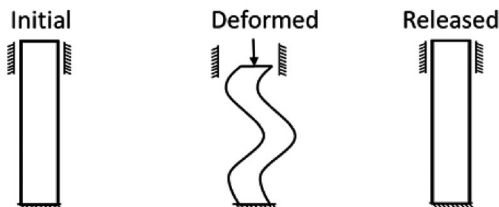
The vibration isolation of a machine part or structure can be achieved by employing three types of systems, and each system isolates the excitation using a specific technique, namely

- i. *Passive control system*—The passive systems work by shifting the system's natural frequency away from the desired working range. It is achieved by adding mass, changing stiffness values, and applying layers of damping material. This method often causes the decaying of vibrations, so they are mostly used for vibration suppression [35].
- ii. *Semi-active control system*—This system is based on the controller's feedback response, where the required command signal is generated. This command signal is used for the real-time adjustment of stiffness and damping for shifting the natural frequency away from the excitation frequency range to obtain the vibration isolation [36].
- iii. *Active control system*—This system uses sensors to detect the vibration signal and actuators to generate

a) Slender elements, sharps and creases



b) Elastic beams



c) Constrained beams

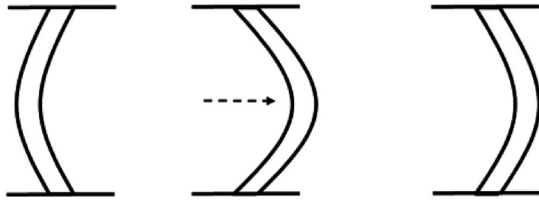


Figure 3. Building block of a mechanical metamaterial. (a) Localize bending. Example—Origami, kirigami inspired metamaterial. (b) Buckling of the beam. Example—stretch dominated metamaterial. (c) Constrained beams with snap-through behavior under buckling [28].

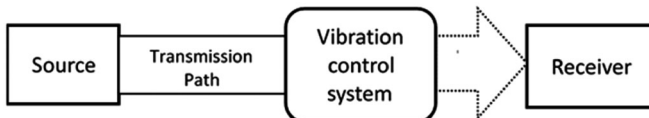


Figure 4. Schematic diagram of a vibration control system.

negative vibration [37]. An external source powers the actuator to impart necessary force and motion to develop a vibration in the opposite direction to cancel the undesired vibrations generated in the structure. The active control system uses actuators, sensors, active controllers, and signal controlling devices to obtain vibration isolation in the desired range [33, 38].

As compared to the active control system, a passive control system is simple and doesn't need any complex control system. Passive control also gives the freedom to attach an unpowered external device to the structure to change the structure's physical parameters for obtaining the desired vibration suppression. Because of these characteristics of passive control, it is preferred over the active control system. A machine or structure is generally designed using static models. The dynamic response is accounted for by considering the factor of safety, as dynamic modeling is more complicated and incurs high computational cost [32]. Due to these practical limitations on dynamic modeling, the machine or structure is provided with a vibration control system after the structure's initial design to mitigate the dynamic response. However, the generally used passive vibration control systems are effective for frequencies higher than the system's natural frequency. The passive system faces limitations in isolation at the low-frequency range

[39]. Hence there is a need for a vibration control system, which has wide frequency bandwidth.

Further, it is also desired to integrate the vibration control system with the structure, so a separate system for vibration isolation can be minimized. The metamaterials can be preferred in these applications because the vibration absorbers are embedded into the main structure rather than attached as an add on device. Further, these vibration absorbers can be designed to generate excellent vibration suppression in wide bandwidth and at low-frequency ranges by varying the physical parameters of the structure [40].

Passive isolation means that the shock isolation depends on elastic supports, the most common devices for shock isolation being helical springs, wire rope springs, elastomers, and pneumatic springs. The effect of passive damping on the shock response can be negative in terms of the peak acceleration; however, damping is still necessary to reduce residual vibrations. Due to the nature of shock excitation, i.e., large displacements and accelerations, the use of nonlinear isolators common, and much work have been devoted to developing mathematical models and experimental devices based on the nonlinear properties [41]. The use of nonlinear isolators is one of the preferred alternatives for shock isolation compared to semi-active strategies. Even though the latter has good performance, they are costly and require more instrumentation [42].

The external passive vibration control system faces limitations in providing isolation of large structures against low-frequency vibrations in terms of the size and mass of the structures. The energy dissipative components such as viscoelastic materials, springs, soft materials, and hydraulic dampers are commonly used in the traditional passive isolators to implement passive vibration control. But these passive energy dissipative components are influenced much by temperature [43]. Further, these control systems are mostly linear in type, and hence they have narrow isolation frequency bandwidth that faces limitations in providing isolation of large structures against low-frequency vibrations in terms of the size and mass of the structures. These limitations can be overcome by using metamaterials, which can be embedded into the structure with a unit cell having stopbands in the desired frequency range. Further, the unit cell can be designed with nonlinearity to achieve broad isolation frequency bandwidth. Further, with metamaterials, the vibration energy of the system can also be harvested, which can be beneficial [44]. Metamaterials are modeled by arranging the microscopic elements periodically to achieve a unique wave propagation behavior to give negative effective properties that generate stopbands; moreover, this stopband favors the use of metamaterial for vibration control purposes [45].

Studies also focus on the class of metacomposites that combines two different aspects of vibration reduction. First is the concept of periodic structures and the second one is to control the mechanical behavior of structures using smart materials. The work about periodic structures is presented in the context of elastic wave filtering called phononic crystals. The waves propagate inside the periodic arrangement of media, and due to the interference phenomenon, there is

diffraction that changes the dispersion properties of waves [46]. The position of the Bragg bandgap is directly related to the spatial arrangement of the crystal. Still, this approach is quite limited for practical applications in which the wavelength is in the range of centimeters or meters. One of the efficient ways to eliminate this constraint is by using locally resonant unit cells. In this approach, the bandgap is opened around the resonance frequency zone of the unit cells, which can be tuned by changing the resonator's mass or stiffness [47].

Although the above mentioned passive approaches are very helpful in broadening the field of mechanical metamaterials for vibration reduction, they have a certain limitation that their geometry cannot be altered after being manufactured. This limitation conflicts with the demands of metamaterials that can be adaptive in nature through some external means and lead to the development of active metamaterials with controllable properties [48–51]. The properties are controlled by means of using smart materials and piezoelectric elements with shunted networks for the wave propagation and tuning stopband in the desired frequency ranges.

3. Bandgap mechanism for the mechanical metamaterials

The mechanical metamaterials can be developed by making some mechanical sub-units or structures inside the main building block so that the mechanical waves transmitting into the building block can resonate with the sub-units of the structure. The properties that generate because of the local resonance results in the existence of a phononic bandgap, known as a stopband. In this stopband, no-wave can propagate inside the building block within that frequency range [52]. Many new models have been designed to increase the position and the bandwidth of the stopband so that the vibration can get isolate for varying frequency ranges.

There are two approaches to study the stopbands characteristics:

- Brag scattering approach: In this approach, there are zones with the destructive interference between reflected and transmitted waves, which results in high reflection and low transmission,
- Light bending approach: This approach depends on the discrete electronic states of atoms and molecules; the waves reflect because of the localized modes or localized resonance.

The mechanism behind these two approaches for wave attenuation is discussed [53]. In the mechanical field, the bandgap formation is achieved by two different mechanisms, i.e., Bragg Scattering (BS) and Local Resonance (LR). The Bragg Scattering mechanism depends upon the periodicity and the lattice constant of a unit cell. The bandgap obtained using the BS criterion limit its use for low-frequency region, as the frequency varies inversely with the lattice constant,

$\nu = c/(2a)$ where ν , c , and a are frequency, speed of sound, and lattice constant, respectively [54]. So, to obtain the low-frequency bandgap, a large value of lattice constant is required, which is not feasible with the increase in demand for small-sized structures. Further, to remove this barrier, Liu et al. [16] proposed a novel idea to achieve wave attenuation at low-frequency sub-wavelength regions using the Local Resonance (LR) mechanism.

The LR mechanism induces the low-frequency bandgap with lattice constant several orders smaller than the wavelength of propagating waves. The bandgap and bandwidth phenomenon generated due to the LR mechanism depends upon the geometric parameters and material properties of resonators; it does not depend upon the periodicity and arrangement of unit cells [55]. The LR mechanism generally consists of a spring-mass system whose natural frequency depends upon the stiffness and mass of the system $(\omega)_n = \sqrt{k/m}$. For low-frequency vibration isolation, either the mass needs to be very large, or the stiffness needs to be small; a resonator is constrained with the heavy mass or small stiffness. Hence to overcome this limitation, several designs have been proposed throughout the years for utilizing the fascinating properties of mechanical metamaterials for vibration control.

The active metamaterial approach is the other way to add a resonant system to the structure without modifying the original design by using piezoelectric patches shunted with RL circuits. The tunable characteristics of shunted piezo-patches allow the equivalent impedance of the structure to be tuned to the desired frequency ranges to generate stopbands [56]. Damped resonance is generated in the shunt circuit due to the presence of resistance; this resistance dampens the vibration amplitude outside the stopbands. However, the main limitation of this shunted-piezo circuit is narrow-band effectiveness. This limitation can be overcome by using negative capacitance shunts [57]. By tuning this negative capacitance in accordance with the effective capacitance of the embedded patch, the total impedance of the shunt circuit can be reduced to that of the remaining circuits. Active control is another way of tuning structural properties by varying the parameters of smart material. Some parameters like inducing impedance can tune the dynamic stiffness, the negative capacitance can tune Young's modulus, etc. This opens the way for the frequency-dependent effective impedance that can be tuned to the desired frequency ranges for generating stopbands. The adaptive characteristics of electrical shunts can be a very efficient way to force the waves to follow the path of interest that leads to vibration reduction, energy harvesting, etc. [58].

Mechanical metamaterials used for vibration control are designed based on the requirements such as space constraint, type of material, type of applications, etc. In this review, the mechanical metamaterials are sub-divided into passive metamaterials and active metamaterials. Moreover, the designs that are discussed in the subsequent sections use metamaterials as the main ingredient for controlling the vibration.

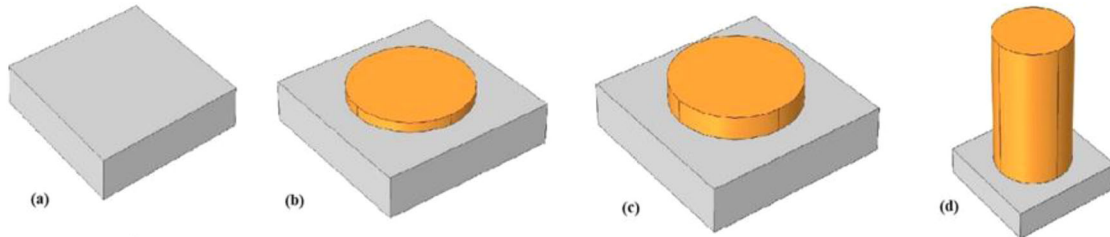


Figure 5. (a) Thin aluminum plate with thickness $h_1 = 1$ mm, (b) stub height $h_2 = 0.25 h_1$, (c) stub height $h_2 = 0.5 h_1$, (d) stub height $h_2 = 10 h_1$. The lattice constant $a = 10$ mm, diameter of cylinder stub = 7 mm. [60].

4. Vibration control using passive metamaterials

The vibration control can be achieved by designing the metamaterials in certain ways based on the constraints such as space, materials, and desired isolation range. Four different criteria are discussed in this section.

4.1. Vibration control using thin metamaterial plate

The phononic crystal bandgap has been studied under the bulk waves and surface waves for the steel/epoxy phononic crystal plate [59]. However, the wave attenuation has been limited to the mid-high frequency range because the wave attenuation was analyzed by the Bragg scattering criterion. Wu et al. [60] performed phononic bandgap analysis for the low-frequency wave attenuation on a thin aluminum metamaterial plate with varying stub height over it, as shown in Figure 5. They performed the numerical simulations for the bandgap in COMSOL multiphysics software and validated with an experimental study. They studied different stub height over the aluminum plate and found a wide bandgap at the stub height three times the thickness of the metamaterial plate.

Zhu et al. [61] performed both experimental and numerical studies on the thin metamaterial plate with periodic cantilever mass structures for both in-plane and out-of-plane guide waves for low-frequency applications. Five different shapes of unit cell structure were studied such as (i) Unit cell in a thin metamaterial plate with internal square cutout, (ii) an interior cantilever beam is added in the unit cell, (iii) a mass (m_1) is added to the tip of a cantilever beam in the unit cell, (iv) a mass ($m_2=2m_1$) is added to the tip of the cantilever in the unit cell, (v) a mass ($m_3=3m_1$) is added to the tip of the cantilever in the unit cell as shown in Figure 6(a)–(e) respectively. Stainless steel was used as the material for the analysis of plate that has thirty-unit cells along the length and two-unit cells along the width; the spacing of the adjacent unit cells are taken as 5.6 mm, and thickness as 1 mm. The numerical simulation was performed in ANSYS software, and the results showed no low-frequency bandgap for the first two-unit cells (i.e., for Figure 6(a) and 6(b)). The low-frequency bandgap was observed for the unit cell containing mass at the tip of the cantilever; the bandgap gets lowered as the mass increases on the tip of the cantilever. This lowering can be justified by the resonance mechanism of the beam, where resonance frequency is estimated by $\omega = \sqrt{K_{eff}/M}$. M is the mass at the tip.

Lu et al. [62] designed two new metamaterial plates (Figure 7), having an irregular local resonance system on the aluminum plate for Flexural Vibration Bandgap (FVBG) in the low-frequency ranges, and validated the bandstructure with the transmission curve using numerical simulation. The unit cell is constructed by placing a local resonant structure on the aluminum plate (green part); two different resonators are made separately on the aluminum plate. The first resonator consists of a wedge lead mass (gray region) placed on a rectangular silicon rubber plate (yellow region), called a wedge mass elastic metamaterial plate (WMEMP). The second resonator (Figure 7b) consists of a rectangular lead mass (green region) placed on a wedge silicon rubber plate (gray region), called a wedge rubber elastic metamaterial plate (WREMP). For WMEMP, the dimensions of the wedge mass are $(h_1+h_2) \times b \times a$, silicon rubber plate is $b \times b \times h_3$, rectangular plate is $a \times a \times e$, as shown in Figure 7(a). For WREMP, the dimensions of mass are $b \times c \times h_6$, silicon rubber plate is $(h_4+h_5) \times b \times a$, rectangular plate is $a \times a \times e$, as shown in Figure 7(b). The dispersion curve was plotted for both the samples, and then the mechanism of FVBG formation was analyzed using the displacement field of eigenmodes and effective mass density. This study identified two resonant frequencies, which are associated with the torsional vibration of the local resonant mass along a different axis. Negative effective mass regions are also observed on both sides of the resonance frequencies, which is due to the inhomogeneity of the wedge mass or rubber. This negative mass region leads to two low-frequency FVBG for the unit cell. The parametrical study was also performed by varying only the height of the mass and rubber plate, maintaining the weight of the system constant. It was concluded that, as mass increased, the upper FVBG moved toward the lower frequency range with broader bandwidth, and the lower FVBG also moved toward the low-frequency range but with constant bandwidth.

Li et al. [63] designed a sandwich-like metamaterial plate consisting of mass-beam resonators (Figure 8) to obtain vibration isolation at low-frequency ranges. The dispersion curve was obtained by analytical and numerical techniques, and it was further validated by the transmission loss curve obtained using both experimental and numerical techniques. The structure consists of two flat plates fixed by supporting rods and resonators. The resonator consists of a cantilever beam and a mass block that is fixed on the supporting rod, as shown in Figure 8. The mass of the supporting rod is added to the flat plate, and the stiffness of the supporting

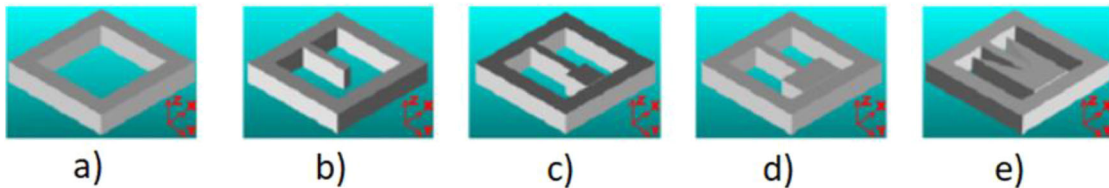


Figure 6. Different designs using plate (a) unit cell containing only square cutout, (b) unit cell with added interior cantilever, a unit cell with added tip mass (c) m_1 , (d) $m_2=2m_1$, (e) $m_3=3m_2$. [61].

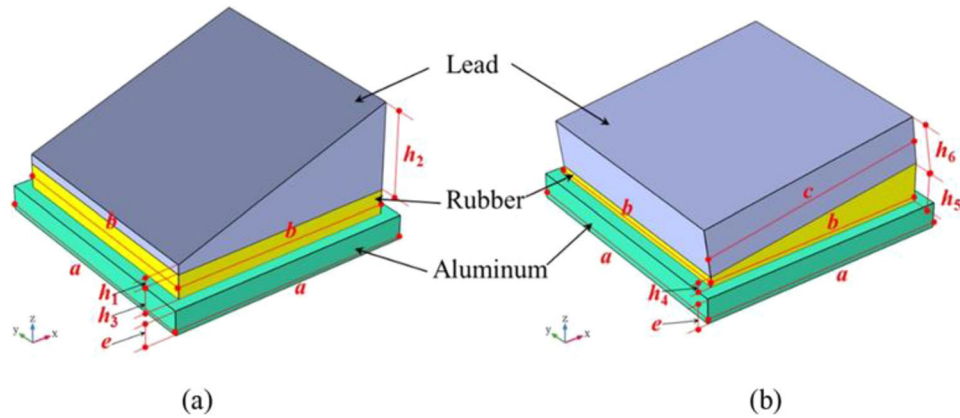


Figure 7. Unit cell for metamaterial plate (a) wedge mass, (b) wedge silicon rubber [62].

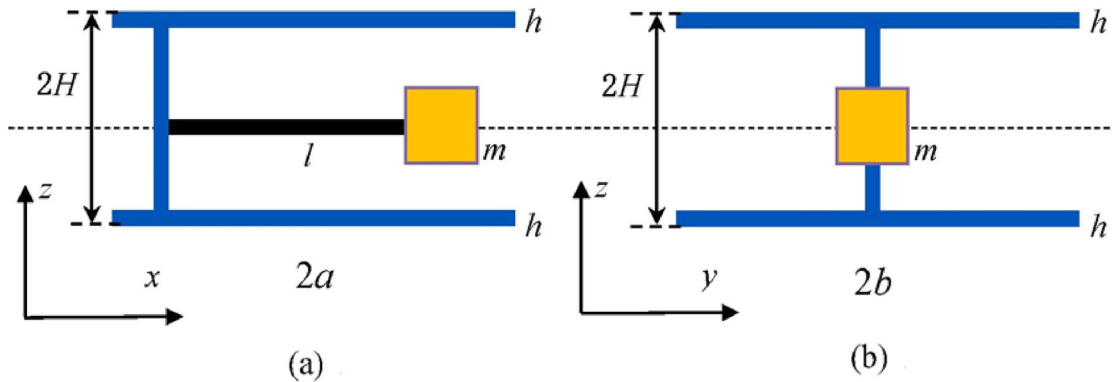


Figure 8. Unit cell of metamaterial plate (a) front view, (b) side view [63].

rod is considered infinite during the calculation. In the analysis, it is assumed that the mass of the block is much larger than the cantilever beam, and the bending moment of the cantilever beam is much larger than the mass block. Therefore, the bending potential energy of the mass block and kinetic energy of the cantilever beam is ignored. The conservation of energy method is used to obtain the dispersion relation to determine the stopbands analytically. The study observed that the stopband can be adjusted by varying the mass ratio of resonators and faceplates and also by altering the natural frequency of the resonator; the width of the stopband can be increased by considering a large damping ratio. The results showed transverse mechanical wave attenuation at low-frequency ranges due to the natural frequency of the resonator. The transmission loss curve is also plotted by considering 10×5 unit cells along the faceplate. Vibration attenuation was observed at the stopband, which validates the bandgap obtained from the dispersion curve.

He and Huang [64] developed a new metamaterial plate for the wave attenuation in varying frequency ranges, as shown in Figure 9. The unit cell consists of a resonator installed inside a rectangular hole on a rectangular metaplate. The resonator consists of a mass placed at the center attached with the springs on top and bottom. The resonator is installed into the rectangular plate with the help of four trusses, two trusses on the top and two on the bottom. Both the pairs of trusses are placed orthogonally, as shown in Figure 9. They developed the analytical model and further compared it with the numerical simulation results. The result showed wave attenuation in the low-frequency region. The parametric study was also performed based on the variation of material properties and geometric parameters. It is found that by increasing the mass of the resonator, the bandwidth increases, and the bandgap frequency moves to a lower range; on the other hand, by increasing the stiffness of the springs, the bandwidth also increases but the bandgap

move toward a higher range. By changing the geometrical parameters of the plate, the lower bound frequency of the bandgap showed little effect. Still, the upper bound frequency of the bandgap increased, resulting in the wide bandwidth.

In another study, acoustic-based two visco-elastic metamaterials are developed for the vibration isolation applications [65]. The first acoustic metamaterial consists of an array of split-hole spheres (SHS) acting as a Helmholtz resonator, which can be used for the effective tuning of the bulk modulus of acoustic material to generate bandgap. The design consists of a triangular porous mesh that contains seven SHS in a triangular array, as shown in Figure 10(a). The resonant frequency of the Helmholtz resonator is given by

$$\omega_0 = C_0 \sqrt{\frac{S}{L' \cdot V_r}} \quad (2)$$

Where C_0 is the ambient sound speed, S is the cross-sectional area of the neck, L' is the effective length of the neck, V_r is the volume of air within the cavity. Equation (2) shows that the resonance frequency of the resonator can be

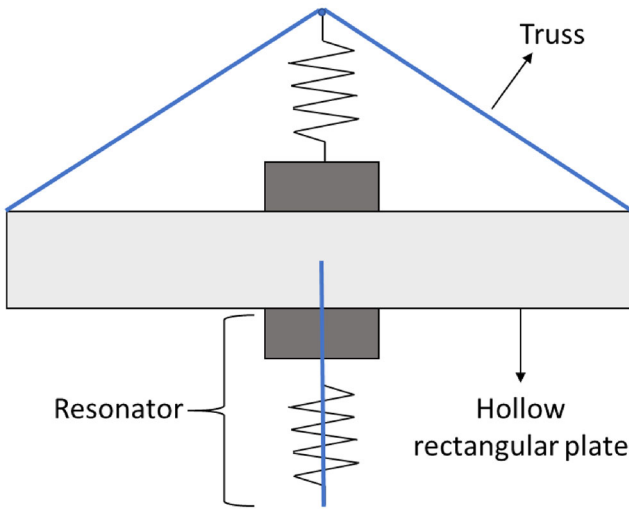


Figure 9. Schematic view of the unit cell [64].

controlled by varying the parameters of SHS, which can be used for further tuning of effective bulk modulus property to generate the bandgap at low frequencies. The second acoustic-based metamaterial, shown in Figure 10(b), is designed with a double negative behavior to achieve the low-frequency bandgap. This metamaterial is developed based on the lumped parameter analogy with additional stiffness using the viscoelastic elements. This design approach induces the double negative behavior that is required for the vibration isolation application. Further, the architecture of SHS can be suitably designed to achieve the bandgap in the desired frequency range.

4.2. Vibration control using micro-structured metamaterial

The unusual properties of the metamaterial are derived from the rationally designed microstructures rather than the properties of the base material [28]. Thus, the orientation, shape, and size of the internal microstructure can be designed to create exceptional mechanical properties. Aghighi et al. [66] developed a new design of microstructure for low-frequency bandgap by fabricating small periodic microstructures of length scale lesser than 1 cm (≤ 1 cm) as shown in Figure 11. The structure consists of a periodic unit cell with a total volume of 1 cm^3 , the total thickness of the structure was taken as 6 cm. It was designed for bandgap attenuation in longitudinal frequency mode ranging from (0–5 kHz) precisely 3 kHz. The bandgap property was achieved by the inclusion of locally resonant material having low natural frequency inside a hollow polymer cavity. The unit cell consists of a 3D structure with mass-spring inclusions for resonance, and two geometries are studied for different combinations of resonator design. The first hollow unit cell has 1 mm wall thickness, and T shaped resonator (with head mass and cantilever bending stiffness) was designed for the longitudinal resonance mode around 3 kHz. The second hollow unit cell has 1.5 mm wall thickness, and H shaped resonator was designed to have a wide-bandgap around 3 kHz. Eigen frequency analysis is performed for both the unit cell (with

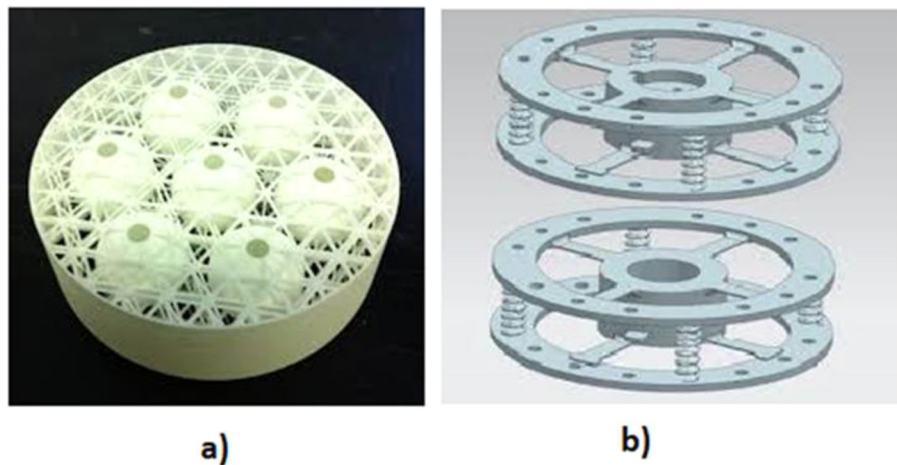


Figure 10. (a) Acoustic metamaterial with a triangular porous mesh consisting of a hexagonal array of 7 SHS, (b) CAD representation of visco-elastic metamaterial for vibration isolation [65].

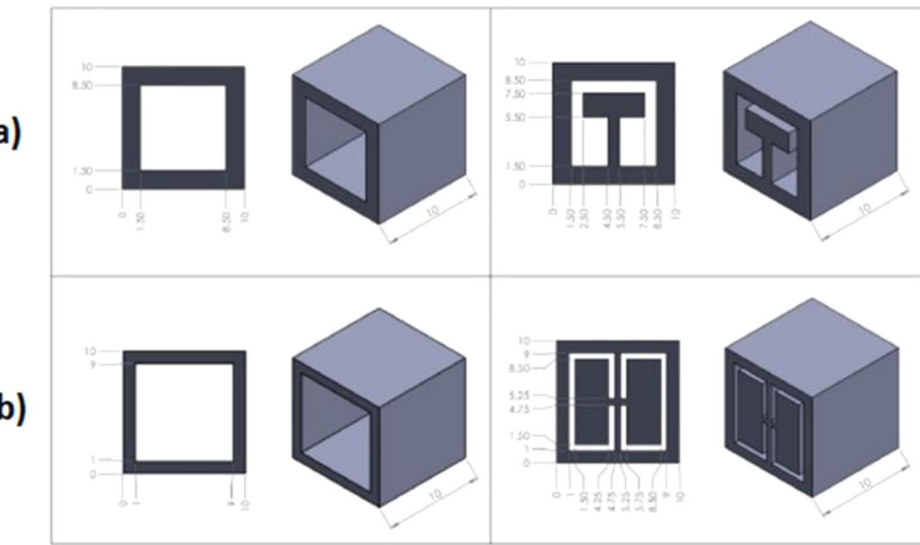


Figure 11. (a) Hollow unit cell with wall thickness 1 mm, and unit cell with T shape resonator inclusion, (b) hollow unit cell with 1.5 mm unit cell thickness, and unit cell with H shaped resonator inclusion [66].

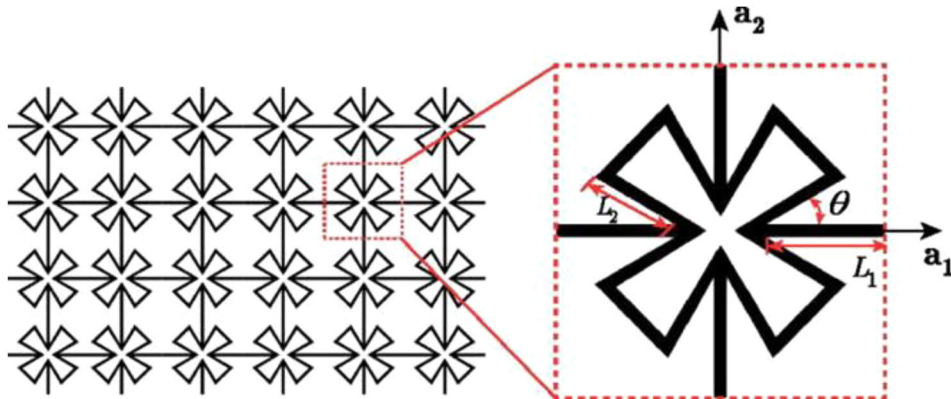


Figure 12. Divergent star-shaped unit cell with the geometric configuration [67].

and without the resonator) using Bloch-Floquet boundary conditions in COMSOL Multiphysics software to get the band structures of all the cases. An experimental study was also performed by fabricating the unit cell in arrays to validate the numerically obtained results. Finally, the unit cell was optimized for the low-frequency stopband for longitudinal modes of vibration.

Nitish and Siladitya [67] proposed a new metamaterial for the wave attenuation in a low-frequency range. The unit cell consists of three different star-shaped designs based on the angle between the adjacent cell walls, i.e., θ , as shown in Figure 12. The proposed three different star-shaped designs are (a) Divergent shaped star, where $\theta \in [25^\circ, 45^\circ]$, (b) Crossed shape star, where $\theta = 45^\circ$, (c) Convergent shaped star, where $\theta > 45^\circ$. These unit cells are arranged periodically in an array and numerically obtained the dispersion curve to determine the bandgap of the unit cell. The sample was manufactured using a 3D printing technique. Further, the transmission loss study was conducted to obtain the FRF graph both numerically and experimentally. This transmission loss curve was used to validate the bandgaps derived from the dispersion curve. A parametric study was also

performed by varying the length of divergent ribs (L_2) and θ . With the increase of L_2 keeping θ constant, the bandgaps got enlarged because of the decrease in the discontinuities. But as θ increases, keeping the L_2 constant, the effective mass reduced that shifts the bandgap to high-frequency range, the optimum result was obtained at $\theta = 30^\circ$. It was concluded that the lightweight divergent shaped unit cell structure attenuated the mechanical waves at the low-frequency region with enhanced bandgap.

Elmadih et al. [68] designed a new metamaterial having cubic unit cell with the Face centered struts and reinforcement struts in x, y, and z directions (FCCxyz), as shown in Figure 13. They studied the 3D elastic wave propagation to evaluate the vibration isolation at a low-frequency range. The Face-centered struts provide good compressive strength to the unit cell consisting of an internal resonator. The internal resonance mechanism is achieved by mass supported by the six-struts that provides stiffness. These six struts are attached to the mass on one end and to the inner walls of the FCCxyz unit cell on the other end, as shown in Figure 13(a). The stiffness of the resonator increases with the increase in strut diameter, and the volume fraction gets

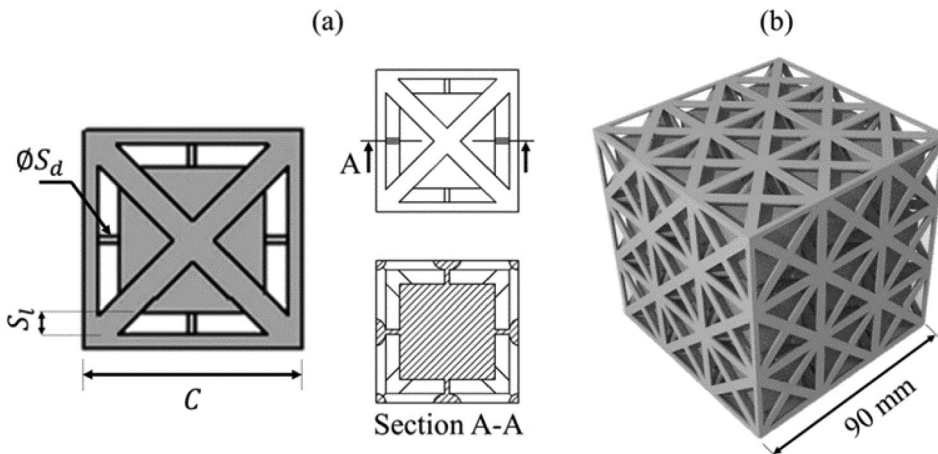


Figure 13. Design of resonating metamaterial (a) sectional view of the Unit cell, (b) an array of $3 \times 3 \times 3$ unit cells [68].

altered by the strut length, i.e., less strut length means a large size resonator. The FEM simulation results showed that the large size resonator has a stopband at a low-frequency range and also wider bandwidth than the medium and small size resonator. The bandgap is found at a range much below than that obtained from the Bragg scattering mechanism with a similar size. Further, the sample was fabricated by Laser Powder Bed Fusion (LPBF) method and was tested experimentally for the transmission loss curve to validate the results obtained from the numerical simulation.

D'Alessandro et al. [69] designed a new metamaterial for controlling the mechanical wave propagation in the low-frequency region using the separation of modes principle. This principle relies on the specific arrangement of the elements that consist of mass and elastic ligaments. The unit cell is designed in the sub-wavelength dimension and consists of a periodic arrangement of pyramid masses and elastic ligaments, as shown in Figure 14. The elastic ligaments provide the stiffness, and the structure acts as a resonator. The additive manufacturing technique (Selective Laser Sintering technique) is used for the construction of 2 different samples of 3×3 -unit cells with 3 cm and 5 cm lattice constant, respectively. The numerical analysis was performed to obtain the dispersion curve to analyze the bandgap formed due to the resonance of the unit cells. They conducted a transmission loss study both numerically and experimentally for validating the obtained bandgap. This design has an ultrawide bandgap at a low-frequency range with the maximum incident wavelength quite larger than the unit cell dimensions, i.e., 55 and 33 times for the 5 cm and 3 cm lattice constant samples, respectively.

Another interesting application of metamaterials in vibration reduction through the periodic arrangement of trees is demonstrated by Liu et al. [70], as shown in Figure 15. The trees that are arranged periodically acts as a natural metamaterial. The resonance generated by the trees couples with the Rayleigh waves in the soil to suppress the Rayleigh wave propagation at specific frequencies. The attenuation of the waves at these frequencies leads to the bandgap. This bandgap gets affected by the soil elastic modulus, trunk radius, tree height, and tree spacing. Figure 15 demonstrates

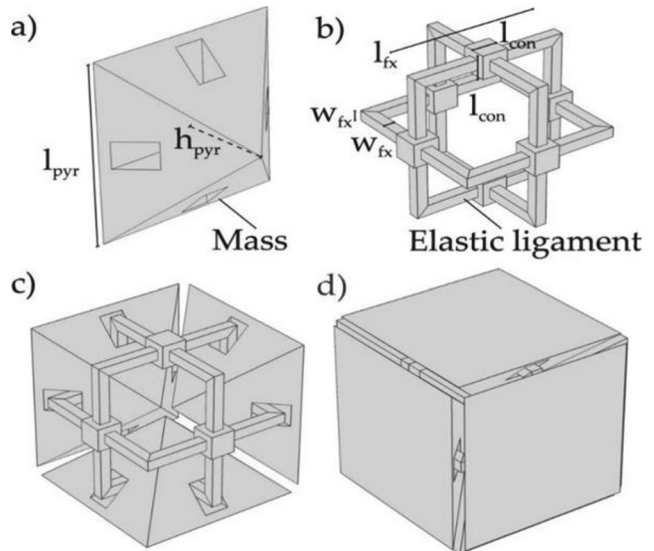


Figure 14. Unit cell description—(a) pyramid mass with geometrical configuration, (b) elastic segment with geometrical configuration, (c) partial composition of the unit cell, (d) final composition of the unit cell [69].

the cause of Rayleigh waves and their suppression by the trees. The surface band gap is also studied by the sound cone method and strain energy method; the results showed that for wider and low-frequency bandgap, the soil modulus should decrease, trunk diameter should be large, tree spacing should be small, and the tree height should increase. The human-made array of trees can induce stopband even up to the frequency of 80 Hz; the most beneficial way for a low-frequency bandgap is by increasing the tree height. In this analysis, only the trunk of the tree was considered for the analysis, as it bears 80% of the weight.

4.3. Vibration control using quasi-zero-stiffness metamaterial

Vibration isolation is essential for all the engineering systems to mitigate the vibrational response of the system to external excitations. When the external excitation frequency is low, then the natural frequency of the system needs to be

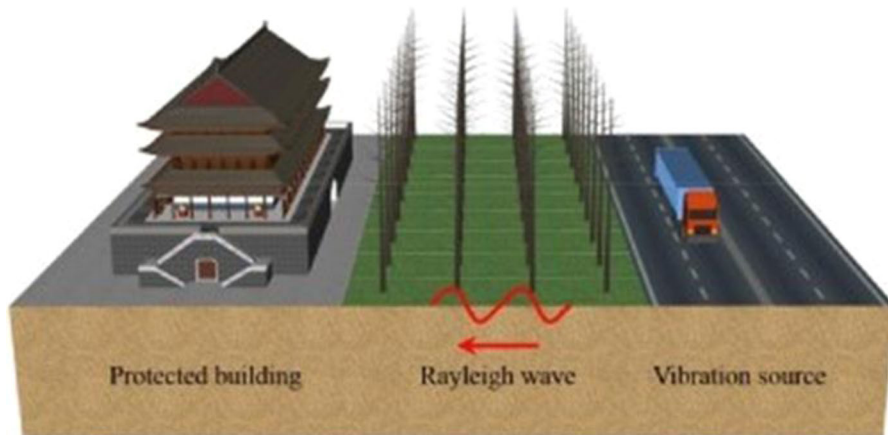


Figure 15. The cause of Rayleigh waves by traffic vibrations and vibration suppression by the trees to protect the Rayleigh wave from reaching the building [70].

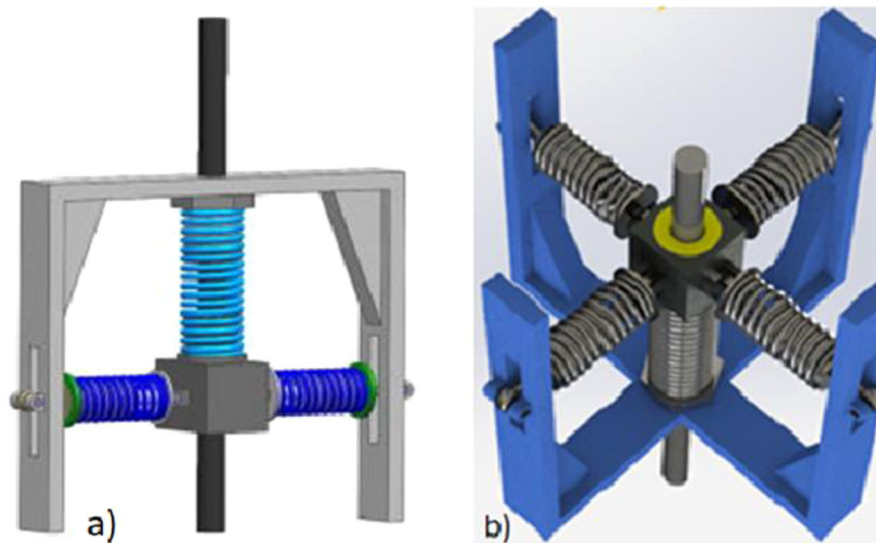


Figure 16. (a) Schematic diagram of HSLDS resonator with three springs for LR-beam [74], (b) Schematic diagram of HSLDS resonator with four vertical spring [75].

reduced by lowering the stiffness (K) of the isolator [71]. However, such a requirement faces limitations that the isolation system also should support the mass of the system. Hence at low frequencies, the linear system suffers a drawback [72]. This limitation of the linear isolation system can be overcome by using a nonlinear isolator having High Static and Low Dynamic Stiffness (HSLDS), also known as Quasi-Zero Stiffness (QZS) characteristics [73].

The high static stiffness provides a large weight-bearing capacity, and low dynamic stiffness provides isolation from low-frequency excitations. This QZS is achieved by introducing a Negative Stiffness (NS) mechanism to neutralize the positive stiffness. The need for QZS encouraged researchers to develop various mechanisms to achieve QZS. The concept of metamaterials for the QZS mechanism is a recent and upcoming field of research. In metamaterial, a unit cell can be suitably designed to exhibit QZS characteristics having nonlinear force-displacement relations.

Zhou et al. [74] used HSLDS resonators in an LR beam to attenuate the flexural waves in a low-frequency zone. The resonator was constructed by using one vertical spring combined with the two horizontal spring orthogonally, as shown

in Figure 16(a). These oblique springs provide the NS mechanism in the vertical direction, which counteracts the positive stiffness of the vertical spring to give the NS mechanism. The mass is suspended by the vertical spring, and these two horizontal springs have no influence on the load-carrying capacity of the vertical spring; Thus, this resonator exhibits high static and low dynamic stiffness values. The net stiffness of the resonator can be tuned by varying the stiffness of the horizontal springs; the resonator is also designed to reduce the nonlinear variation of stiffness under small displacements. Moreover, the bandgap can be tuned to the low-frequency range by tuning the stiffness of the horizontal springs. Further, the efficiency of wave attenuation can be improved by increasing the number of unit cells in the HSLDS-LR beam. It is also concluded that under large excitation, the bandgap becomes narrower by moving toward the high-frequency range, and the wave attenuation efficiency decreases.

In another work, Wang et al. [75] attached HSLDS resonators periodically on a 2D thin beam to analyze the flexural wave propagation in the low-frequency region. The HSLDS resonator consists of a mass attached with a vertical spring

and four horizontal springs, as shown in Figure 16(b). These four oblique springs are evenly distributed and provide the NS mechanism in a vertical direction. The other end of the horizontal springs is connected with the plastic frames, which were further attached to the rib plates to ensure the rigidity of the complete resonator. Under the static condition, the horizontal springs are perpendicular to the vertical spring that supports the whole mass. The stiffness of the resonator is adjusted by varying the stiffness of the horizontal spring from zero to the stiffness value of the vertical spring; different techniques were used to reveal the bandgap structure of the thin beam. The study found that under external excitation, the NS mechanism due to the oblique springs counteracts with the positive stiffness of the vertical spring to give a quasi-zero-stiffness value for the resonator. This novel design is shown to be effective in achieving vibration isolation at low-frequency ranges in the thin beam.

Wang et al. [76] studied the effect of HSLDS resonators arranged periodically in a one-dimensional rod for the attenuation of longitudinal waves. The resonator is constructed by attaching a mass with two horizontal springs and two pre-compressed vertical springs, and the other end of all the springs are connected to the rigid frame, as shown in Figure 17. The resonator is designed to allow the mass to move only in the horizontal plane, and hence the gravity

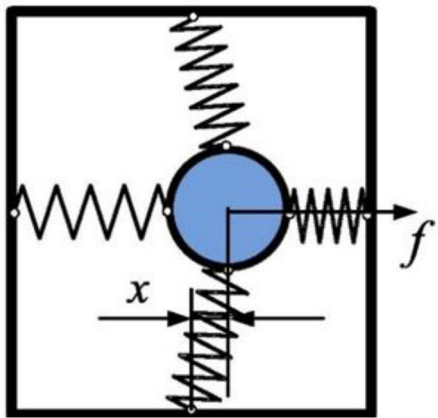


Figure 17. Schematic diagram of HSLDS resonator in deformed configuration [76].

effect can be neglected. Due to this constraint in the design, the vertical springs act as oblique springs to give NS mechanism. When an external force f acts on the mass, the mass gets displaced by distance x in the horizontal direction. Ideally, it can be considered that the stretching of both the horizontal springs is equal and opposite in direction. Under this deformation, both the vertical springs induce NS that counteract the positive stiffness of the horizontal springs to give net QZS value to the resonator. The study concluded that to achieve a low-frequency range bandgap and wide bandwidth, large mass ratio, small damping ratio, and a sufficiently large number of unit cells are required.

Cai et al. [77] proposed a new bistable structure to achieve a negative stiffness mechanism by snap-through behavior, as shown in Figure 18. The unit cell consists of a bistable structure parallelly connected to the elastic element. The bistable structure consists of two pairs of buckled beams, while the elastic element consists of two pairs of multisegmented folded beams (Figure 18). Under compression from the external force, two pairs of folded beams produce positive stiffness, and the two oblique beam exhibits negative stiffness along the longitudinal direction due to the snap-through behavior caused by buckling. In this case, the positive stiffness varies by varying the geometrical configuration of the folded beam; the negative stiffness counteracts with the positive stiffness to produce net QZS for the unit cell. The unit cell is symmetric, as shown in Figure 18. This study found that the QZS behavior causes the wave attenuation in the low-frequency zone; damping leads to increase the bandwidth but lowers the wave attenuation; the bandgap shifts lower with an increase in the mass ratio.

Fan et al. [78] proposed a new design to produce QZS behavior for attenuating the waves in low-frequency regions. The unit cell consists of semi-circular arches undergoing bending dominated behavior, connected in parallel with a sinusoidal beam undergoing buckling behavior, as shown in Figure 19. Under compression deformation, at the initial stage, both the sinusoidal beam and the semi-circular arches show positive stiffness. After exceeding a certain deformation value, the sinusoidal beam experiences snap-through behavior and produces a negative stiffness value to induce the QZS. Therefore, the QZS property of the unit cell

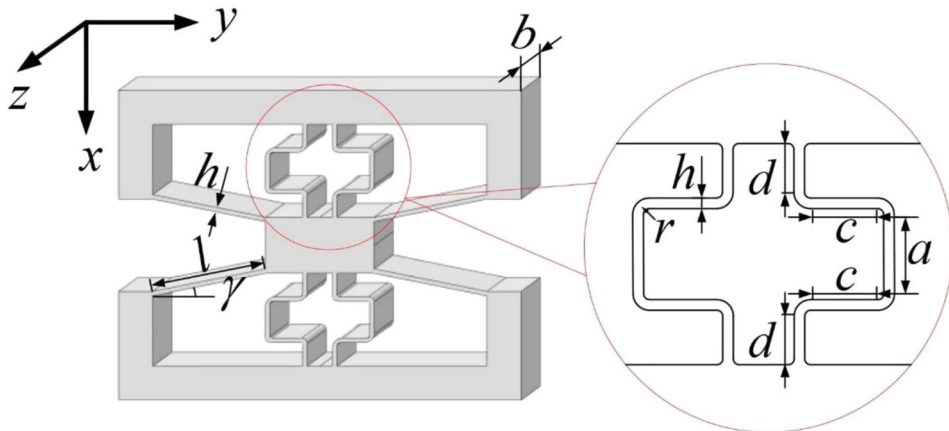


Figure 18. A unit cell of the resonator with the geometric configuration of the folded beam [77].

attenuates the wave in the low-frequency region, and the QZS property can be controlled by varying the designing parameters of the sinusoidal beam and also by pre-loading of the semi-circular arch. It is also identified that this unit cell exhibits better vibration isolation property with a smaller damping coefficient and higher excitation frequency.

Wang et al. [79] designed a semi-active metamaterial beam with an electromagnetic QZS resonator for attenuating the waves in an ultra-low frequency range. The resonator consists of a linear spring that supports the mass of the resonator, a permanent magnetic ring, and a Regulatory Mechanism (RM) consisting of an electrically charged coil and permanent magnetic ring, as shown in Figure 20. During the external vibration, the linear spring experiences

positive stiffness, and the permanent magnetic ring experiences NS that counteracts the positive stiffness to produce the QZS mechanism. The RM is used to regulate the stiffness of the resonator and turn it into an HSLDS resonator. This HSLDS resonator is attached periodically in a beam, and the dispersion curve of this beam is found to exhibit a wide-bandgap in the ultralow frequency zone.

4.4. Vibration control using metamaterial beam with embedded absorber

In beams, transverse waves propagate by shear force and bending moment, and to prevent the wave from moving forward, both translational and rotational absorbers are required. The spring-mass embedded in the metamaterial beam acts as the main local resonator and enables wave attenuation through local resonance. The local resonance can be developed by two methods; negative effective mass and negative elastic stiffness in a beam; both spring and mass effect are there, which can only work as a translational absorber for the dispersive transverse waves.

i. Negative effective mass

The effect of negative effective mass can be demonstrated by considering a two degree of freedom (2DOF) mass in mass system subjected to harmonic excitation, as shown in Figure 21(a). Let $F(t)$ be the excitation force, $u_1(t)$ and $u_2(t)$ be the displacement of mass m_1 and m_2 , respectively, \tilde{m}_1 be the effective mass of m_1 , which needs to be derived. The equation of motion can be defined as,

$$\begin{pmatrix} m_1 & 0 \\ 0 & m_2 \end{pmatrix} \begin{Bmatrix} \ddot{u}_1 \\ \ddot{u}_2 \end{Bmatrix} + \begin{pmatrix} k_2 & -k_2 \\ -k_2 & k_2 \end{pmatrix} \begin{Bmatrix} u_1 \\ u_2 \end{Bmatrix} = \begin{pmatrix} F \\ 0 \end{pmatrix},$$

$$F = F_0 e^{i\omega t}, \quad \begin{Bmatrix} u_1 \\ u_2 \end{Bmatrix} = \begin{Bmatrix} a_1 \\ a_2 \end{Bmatrix} e^{i\omega t} \quad (3)$$

By solving the Eq. (3), Frequency response function H_{11} and H_{21} and the value of effective mass \tilde{m}_1 can be defined as

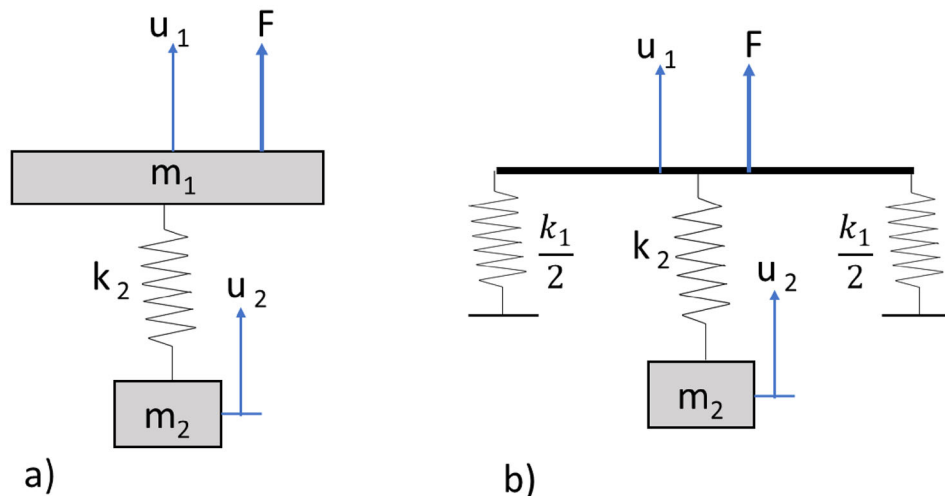


Figure 21. Two degree of freedom systems (a) mass in mass system for negative effective mass, (b) mass in spring system for negative elastic stiffness [80].

$$H_{11} = \frac{a_1}{F_0} = \frac{k_2 - m_2 \omega^2}{(k_2 - m_1 \omega^2)(k_2 - m_2 \omega^2) - k_2^2} \quad (4)$$

$$H_{21} = \frac{a_2}{F_0} = \frac{k_2}{(k_2 - m_1 \omega^2)(k_2 - m_2 \omega^2) - k_2^2} \quad (5)$$

$$\tilde{m}_1 = \frac{F}{\ddot{u}_1} = \frac{F_0}{-\omega^2 a_1} = m_1 + \frac{m_2}{1 - \frac{\omega^2}{\omega_2^2}}, \omega_2 = \sqrt{\frac{k_2}{m_2}} \quad (6)$$

Here ω is the excitation frequency, ω_2 is the local resonance frequency of mass m_2 . There are three tends to infinity, which means $u_1=0$, and the external force is canceled out by the inertial force of mass m_2 through the spring k_2 ; this is the case of

the vibration absorber. (b) When $\omega < \omega_2$, then $\tilde{m}_1 > 0$ then $u_1(t)$ and $u_2(t)$ are in the same phase with each other, and this vibration pattern is known as an acoustic mode. (c) When $\omega > \omega_2$, then $\tilde{m}_1 < 0$ then $u_1(t)$ and $u_2(t)$ are out of phase with each other, known as optic mode, and the effective mass becomes negative [81].

ii. Negative effective stiffness

The effect of negative effective stiffness can be explained by considering a two-degree of freedom system mass in spring system are subjected to harmonic excitation, as shown in Figure 21(b). Let $F(t)$ be the excitation force, $u_1(t)$ and $u_2(t)$ be the displacement of mass m_1 (m_1 tends to zero) and m_2 , respectively, the effective stiffness \tilde{k}_1 needs to be derived, the equation of motion and FRF H_{11} and H_{21} can be defined as-

$$\begin{pmatrix} 0 & 0 \\ 0 & m_2 \end{pmatrix} \begin{Bmatrix} \ddot{u}_1 \\ \ddot{u}_2 \end{Bmatrix} + \begin{pmatrix} k_1 + k_2 & -k_2 \\ -k_2 & k_2 \end{pmatrix} \begin{Bmatrix} u_1 \\ u_2 \end{Bmatrix} = \begin{pmatrix} F \\ 0 \end{pmatrix},$$

$$F = F_0 e^{i\omega t}, \begin{Bmatrix} u_1 \\ u_2 \end{Bmatrix} = \begin{Bmatrix} a_1 \\ a_2 \end{Bmatrix} e^{i\omega t} \quad (7)$$

By solving the Eq. (7), Frequency response function H_{11} and H_{21} and the value of effective stiffness \tilde{k}_1 can be defined as

$$H_{11} = \frac{a_1}{F_0} = \frac{k_2 - m_2 \omega^2}{(k_2 + k_1)(k_2 - m_2 \omega^2) - k_2^2} = \frac{1}{k_1} \quad (8)$$

$$H_{21} = \frac{a_2}{F_0} = \frac{k_2}{(k_2 + k_1)(k_2 - m_2 \omega^2) - k_2^2} \quad (9)$$

$$\tilde{k}_1 = \frac{F}{u_1} = \frac{F_0}{a_1} = k_1 + \frac{k_2}{1 - \frac{\omega_2^2}{\omega^2}}, \omega_2 = \sqrt{\frac{k_2}{m_2}} \quad (10)$$

Here, ω is the excitation frequency, ω_2 is the local resonance frequency of mass m_2 . There are three conditions—(a) When $\omega = \omega_2$, then \tilde{k}_1 tends to infinity, which means $u_1=0$, and the external force is canceled out by the inertial force of mass m_2 through the spring k_2 ; this is the case of the vibration absorber. (b) When $\omega > \omega_2$, then $\tilde{k}_1 > 0$ then $u_1(t)$ and $u_2(t)$ are in the same phase with each other, and this vibration pattern is known as an acoustic mode. (c) When $\omega < \omega_2$, then $\tilde{k}_1 < 0$ then $u_1(t)$ and $u_2(t)$ are out of phase with each other, known as an optic mode, which creates

stopband, and the effective stiffness becomes negative [80, 82].

In another study, Haberman et al. [83] used a spring-mass system to attenuate the transverse wave in a beam. When the dispersed transverse wave propagates into the beam, it leads to a bending moment inducing rotation and a force inducing translational motion in the beam; these elastic waves then resonate the spring-mass system working as an absorber. When this spring-mass system vibrates at optic mode, i.e., at a frequency bit higher than its local resonance frequency, then it creates a shear force and bending moment, which counterbalance the rotational and translational moment caused by the transverse wave and stops the wave propagation (formation of stopband). For longitudinal waves, the negative effective mass indicates the stopband, and for transverse waves, negative effective stiffness indicates the stopband [83].

Early design on using the spring-mass system as embedded absorbed in the beam consists of many numbers of such vibration absorber arranged at a random distance. To study the effect of the arrangement of vibration absorbers in a beam, a numerical study is conducted [84] using the Floquet boundary condition for different cases such as finite beam, infinite beam, and changing the spacing of absorbers. It is observed that for the high-frequency range, the spacing and position of the absorbers do not matter, but for the low-frequency range, the boundary conditions of the beam, spacing, and position of the absorber are critical for the attenuation of waves. [84].

Wu et al. [85] designed a new elastic metamaterial beam with X shaped local resonator for vibration isolation purposes. The numerical and experimental investigations are performed to determine the bandgap and validated it with the transmission spectrum. This X shape mechanism act as a nonlinear resonator that can amplify or mitigate the stiffness of the linear spring attached to the structure. For a linear system, it is difficult to vary the mass or stiffness for changing the natural frequency of the resonator that makes the adjustability of the bandgap even more difficult. On the other hand, the nonlinear stiffness mechanism made it possible to attenuate the waves in varying frequency ranges. In this work, N layers of X shaped resonator have been arranged periodically with unit cell distance L. The X shaped mechanism consists of four rods, four joints, and a horizontal linear spring with stiffness (k_h), as shown in Figure 22. The length of the rods was L_2 and L_1 with length ratio $\beta = L_2/L_1 \geq 1$, and the initial angle of rods was θ_2 and θ_1 , respectively. Hamilton's principle has been used to establish the equation of motion for nonlinear isolators to obtain the dispersion curve and find the bandgap. It was concluded that the local resonator alone possessed weak nonlinearity. However, by taking the equivalent stiffness of the whole metamaterial beam into the analysis, it attenuates the waves in varying frequency ranges by using a nonlinear stiffness mechanism. The parametric study was also performed to amplify or mitigate the stiffness of linear spring, and this stiffness acts as a key feature for the bandgap adjustment. By increasing θ_2 and β , the bandgap shifts toward a higher

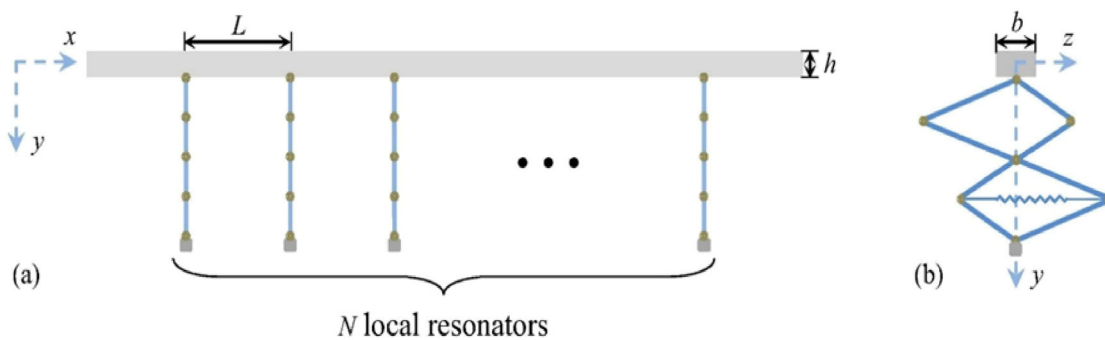


Figure 22. (a) Model of the LR beam with X shaped resonators placed at L distance, (b) geometrical configuration of X shaped resonator [85].

frequency range, and the bandwidth gets broader; by increasing the number of layers N , the bandgap shifts toward the lower-frequency range, and the bandwidth gets narrower.

Vibration characteristics of metamaterial beam embedded with periodic unit cells comprising of built-in local resonant structures are analyzed in [86]. The unit cell consists of a base mass provided with a cavity filled with a viscoelastic membrane to form a local resonance, as shown in Figure 23(a). This resonance enables the wave attenuation at very-low-frequency, ranging from 10 to 5000 Hz. A FEM model is also developed that can be used to study the bandgap characteristics and the frequency response of the beam with a different periodic arrangement of unit cells. Wen et al. [87] studied the vibration transmission and wave propagation in uniform rod with a periodic array of multi-degree of freedom resonators (shown in Figure 23b), numerical results showed both Bragg scattering and resonance type bandgap, the bandgap attenuation can be increased by coupling both Bragg and local resonance type behavior. A chiral metamaterial beam was introduced in [88], the chiral metal composite is introduced with 2D chiral lattice and a cylinder at the core as a metamaterial inclusion for low-frequency wave attenuation (as shown in Figure 23c), with the change in the parameters of the structure double negative mass and stiffness is also found out for some low-frequency range. A finite element study is performed to analyze the vibrational isolation behavior of a beam embedded with only two spring mass-damper (as shown in Figure 23d), and the stopband region was tuned for low-frequency waves by varying the damping ratios of the absorber [89].

In another investigation, Aditya and Karami [90] used deployable structures along with origami-inspired structures as metamaterials for tunability of the wave attenuation. The repeating unit cells consist of a beam/panel connected by a torsional spring (folding mechanism). The wave manipulation was studied based on the folding mechanism by considering two cases: the first one by considering the angle between two adjacent beams (fold angle) as zero, and another by considering fold angle greater than zero. It was found out that by increasing the fold angle to 90-degree, the bandwidth of the four lowest bandgap was increased by 252%, 177%, 230%, and 163% relative to the bandgap at a 0-degree angle. In addition, an increase in the bandwidth of odd number of bandgaps was also found at small fold

angles; the bandwidth of the first and third bandgap gets doubled by increasing the fold angle from 0 to 20 degrees. Transfer matrix formulations found out that only flexural waves propagate at 0-degree fold angle, and both longitudinal and transverse waves are coupled for a non-zero-fold angle. Figure 24 shows solar arrays with adjacent beams connected by a torsional spring. The use of foldable structures found applications in the automotive industry as airbags [91], deployable solar panels [92], foldable telescopic lens [93]. Foldable origami-inspired structures found applications in self-folding robots [94], medical stents [95], etc.

Spadoni et al. [96] investigated the dynamic properties of chiral truss core assemblies for reducing vibration. The chiral topology is among the various geometries with negative Poisson's ratio that features localized deformation when excited at one of its natural frequencies. The resonance can be exploited to minimize the power required for the appearance of localized deformations. Chiral truss-core assemblies are considered to obtain useful deformation shapes because it offers scalable geometry with constant weight. The considered structures are designed to generate deformed shapes, where the deformations are mostly localized in the limited regions of the structure. The nature of these deformed configurations and the freedom provided by the chiral geometry lead to applying the proposed configuration for the design of lifting devices such as airplane wings or helicopter rotor blades. The feasibility of these concepts and dynamic characteristics was investigated by developing a numerical model validated with the experimental results.

In another investigation, Beli et al. [97] used additive manufacturing technology to fabricate metamaterial beam with spatially correlated variability and further investigated its physical effects for wave attenuation. In this study, ten different metastructures were fabricated and analyzed individually and as an assembly as well; their geometric and material properties were tracked, which allowed to obtain a link between the dynamic behavior and spatial variability distribution of the metastructures. The spatial correlative variability in the beam breaks the transitional periodicity and enhance the wave attenuation performance of the metastructures. The study reveals that the vibration attenuation bandwidth widens with the degree of disorder. However, after a certain degree of disorder, the bandgap mistuning causes the wave attenuation to get vanished. In addition, for the forward waves, the variability induces a locally resonant

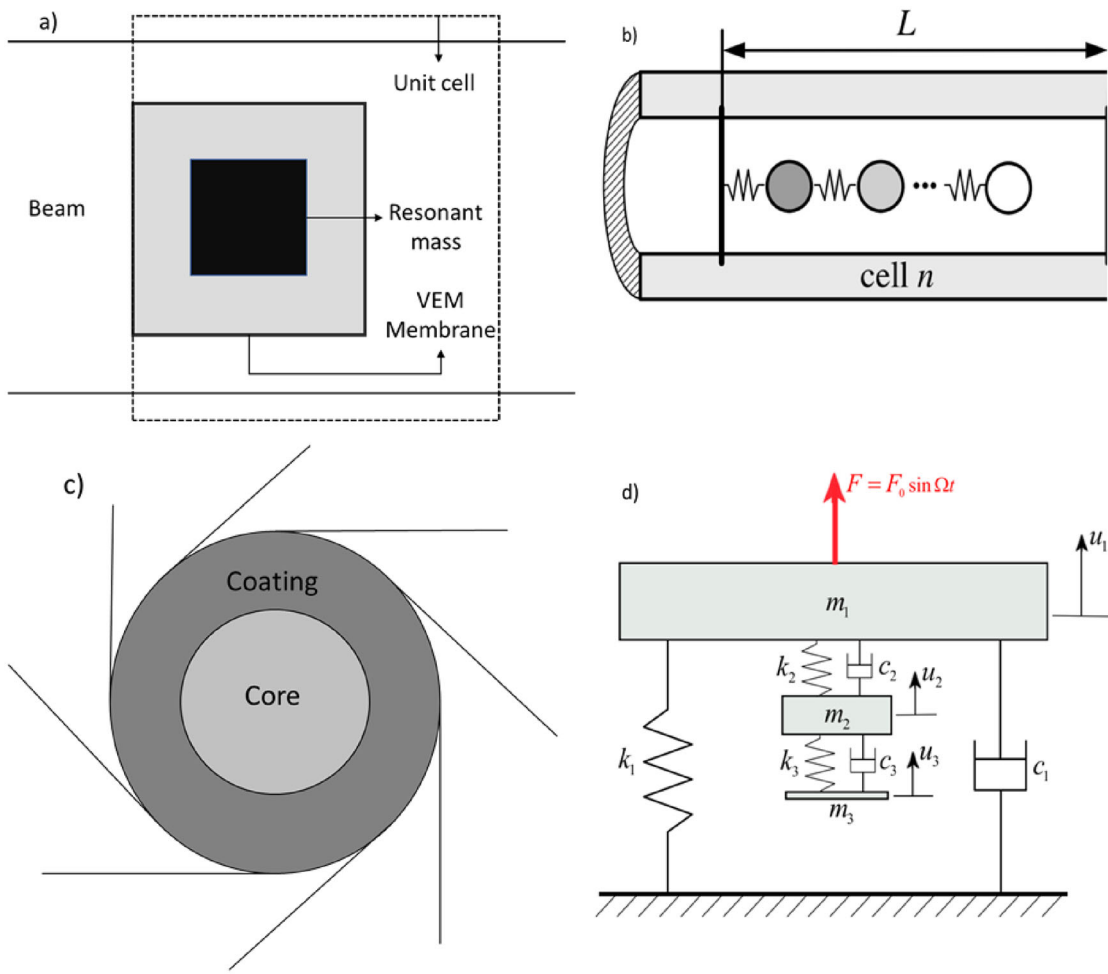


Figure 23. (a) Unit cell consisting of resonant mass with the cavity filled by the VEM membrane. [86], (b) unit cell consisting of MDOF resonators [87], (c) unit cell of chiral meta-composite with a cylindrical core [88], (d) unit cell consisting of two mass spring damper vibration isolators [89].

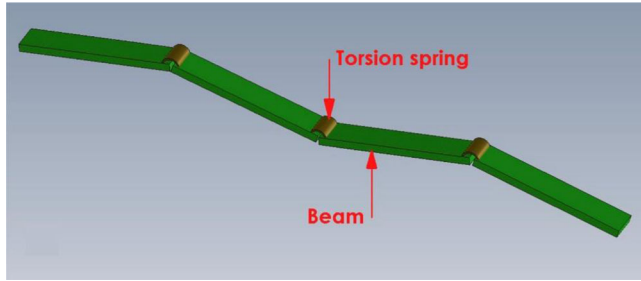


Figure 24. Deployable solar array: Consecutive cells with panels/beams attached with torsional spring [90].

bandgap due to the resonance of the cantilever in mass resonator. This gradually slows down the group velocity to zero and gave rise to a wave trapping phenomenon. A rainbow metamaterial with linear spatial-frequency trapping was proposed based on the wave trapping phenomenon having potential applications in energy harvesting, spatial wave filtering, etc.

5. Vibration control using active metamaterials

Proper designing of the architectures in the targeted frequency zones enables the application of mechanical metamaterials in waveguiding [98], acoustic cloaking [99], and

vibration reduction [100, 101]. The designs discussed in the previous sections used static and passive structures, and also their properties cannot be changed after the fabrication of metamaterials [102, 103]. This limitation lacks the tunability of the bandgaps in the desired range. To overcome this limitation, external mechanical stimuli are used to differ the mechanical properties by changing the geometry either by snapping or buckling [104, 105]. The recent surge in smart structures whose dynamic properties can be changed according to the demand led to the origin of active metamaterials that can change into the predetermined shapes upon excitation by the external stimuli by using shape memory inserts were investigated in [106–108]. The key feature of these metamaterials is their controllable characteristics that are realized by using smart materials. Some of the examples like using Piezoelectric shunt with resonant circuits to obtain tunable stopbands by varying the equivalent dynamic stiffness [49, 109, 110], using electro-magnetic coupling for control in wave dispersion in acoustic interaction [111, 112], tuning stopband by varying directivity of the wave propagation [113, 114], using negative impedances along with piezoelectric circuit to design controllable unit cell [115, 116] and many more.

Active metamaterials generally make use of stimuli-responsive materials like hydrogels [117], liquid crystal

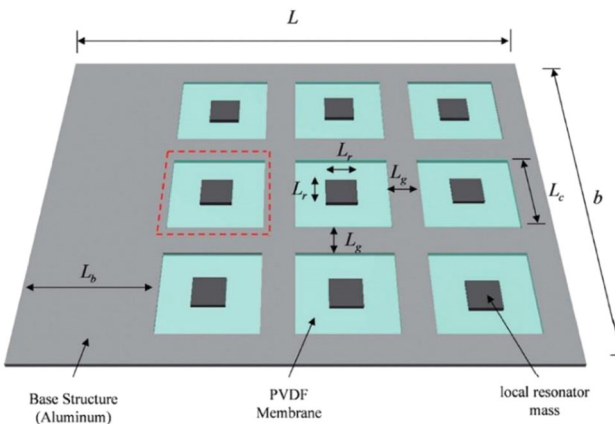


Figure 25. Metamaterial plate with periodic local resonance. PVDF membrane supporting local resonator mass [51].

elastomers [118], shape memory polymers [119] that change their shape and size under external stimulus behavior. When these materials are incorporated in metamaterials, it creates a wide space functionality and potential future applications like soft robotics [120], tunable acoustic metastructures [121], deployable structures [122], etc. For tunability of the properties, rapid and reversible actuation are highly desirable, which is achieved by bending deformation and folding deformations in the case of active metamaterials. In this section, different techniques used for the tunability of bandgaps are discussed. As the active metamaterials can be used for both noise control in acoustic metamaterials, and vibration control in mechanical metamaterials; only the vibration control techniques are discussed.

Nouh et al. [51] examined the possibility of tuning the wave dissipation characteristics of local resonant metastructures by introducing an active element. Local resonances in any periodic structure work as dynamic vibration absorbers of mechanical vibration. The idea behind using multiple Degrees of freedom (DOF) vibration absorbers is to merge the primary single DOF system with multiple secondary systems to reduce the high vibration amplitudes by a significant amount exhibited around the natural frequency of the primary system. Vibration damping over a wide frequency range is achieved by tuning the mass, stiffness, damping ratio of the individual absorbers. The proposed metamaterial plate in this study was equipped with a vibration absorber in the form of local resonators, the dynamic properties of these local resonators were varied by employing an active element to control the location and bandwidth of the local resonance frequencies.

Externally excited piezoelectric polyvinylidene difluoride (PVDF) membranes were used as active elements to host the local resonators. The PVDF films are arranged in a square grid on a host aluminum plate and are used to hold the resonant masses, as shown in Figure 25. These PVDF membranes are excited by an external voltage to exert tensile or compressive in planeloads; this results in stiffening or softening of the PVDF films. The resonance frequencies are controlled and tuned by virtue of this stiffening and softening of membranes. Both theoretical and experimental studies confirmed the presence of stopband and broad bandwidth at

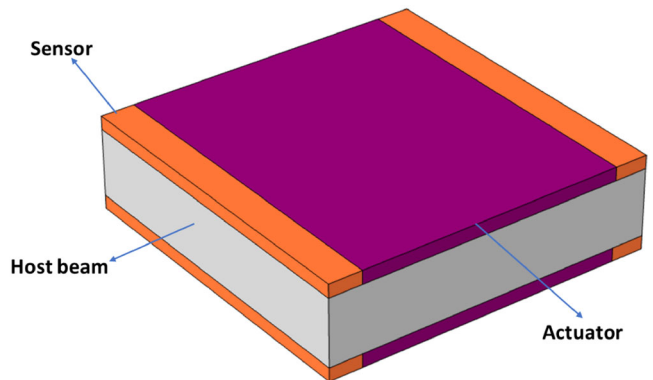


Figure 26. Unit cell of active metamaterial [123].

further low frequencies by the use of the external active element.

Kaijun Yi et al. [123] studied one-dimensional active metamaterial with broadband controllable bending stiffness used to tune the bandgap. The active metamaterial is composed of a host beam with piezoelectric patches bonded on it, as shown in Figure 26. These patches work as sensors and actuators for the closed-loop feedback system. The bending stiffness is controlled using a direct active feedback control law where the voltage on the sensors act as Input and voltage applied on the actuators act as Output. In a control system, the bending stiffness of the active unit is $(1 + \alpha)$ times of that of the bare host beam, α being a design parameter in the control law. The active units are first used in a spatial periodic waveguide to have tunable bandgaps, and then they are integrated into a spatiotemporal periodic waveguide to get non-reciprocal wave propagation. Performances of the two waveguides are studied and compared. In a 1D spatial period waveguide, tunable bandgaps are obtained by softening or stiffening the waveguide. The bandgaps get broadened when the waveguide is softened, and also the first bandgap shifts to low-frequency ranges. The active units are then applied to realize a 1D spatiotemporal periodic waveguide for non-reciprocal wave propagation, where the moving modulation of the local bending stiffnesses is observed by alternating the applied α for each active unit between two designed values. With the use of an appropriate modulation frequency, complete unidirectional band gaps are showed.

Ren et al. [124] proposed a novel elastic metamaterial plate with tunable bandgap characteristics using active control strategies. The piezoelectric actuators and sensors bonded along one direction of the metamaterial plate work as the control system. Displacement and acceleration feedback control methods are employed to provide the positive stiffness and inertia to the plate for active tuning of the bandgap. The study proposed the following results—(a) the displacement feedback control can achieve Ultralow-zero frequency bandgap, and the bandwidth can be enlarged by increasing the displacement control gain, (b) Wide bandgaps can be achieved by the acceleration feedback control, the starting frequency of the first bandgap can be decreased by increasing the acceleration control gain, (c) The displacement control gain can amplify the bandgap at medium and

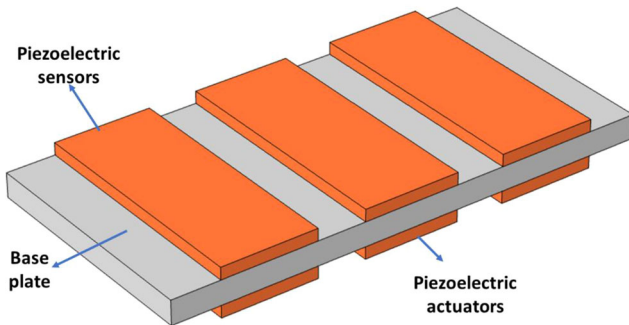


Figure 27. Active metamaterial plate with periodically placed piezoelectric sensors [124].

high-frequency range, and this bandgap can be further enlarged by the acceleration control gain, (d) The width of zero-frequency bandgap and Bragg-type bandgaps can be widened by increasing the thickness of piezoelectric patches and narrower base plates. The proposed elastic metamaterial plate is shown in Figure 27.

Collet et al. [48] used integrated adaptive metacomposites and merged it with the notion of programmable material to allow control over the material physical behavior for vibration and noise control. The concept of metacomposites in this work was to employ it as a shunted piezoelectric smart structure for vibration control and as active acoustic skin for noise control; by the implementation of controlled and adaptive behavior.

An adaptive acoustic liner controls the acoustical impedance (metacomposites) made up of the distribution of individual cells as micro-controller, actuator and sensor, signal amplification, power supply, and signal conditioning. The active skin can be depicted as a distributed interface, where skin displacement $u(x, t)$ is forcefully made the function of fluid acoustic acceleration $\ddot{\omega}$ by a suitable control operator. This acceleration is directly proportional to the measured acoustic pressure. This methodology's main objective is to cancel the positive group velocity of the incident acoustic wave due to its interference with metacomposites. Thus, all incident waves intercepting the adaptive acoustic liner only propagate energy in the negative (x) direction and becomes evanescent for the positive (x) wavenumber component, as shown in Figure 28(a).

For vibration control, a classical approach is used to design adaptive metacomposites to create local resonances by coupling with piezoelectric patches. This involves a periodic array of RL-shunted piezoelectric patches placed on the structure to control the propagation of waves. Periodically induced impedance mismatch zones create a region known as a stopband where waves do not propagate. These shunted piezo patches are tuned to achieve the mechanical impedance of the structure for desired frequency ranges. The metacomposites studied, in this case, is developed by using periodically shunted piezoelectric patches on optimal electric shunt circuits. This optimal electric impedance gives negative capacitance in all conditions and seems to be quasi-constant resistance in series as well. The metacomposites used for the experimental purpose is made of piezocomposite cells connected to specific electrical impedance. The

supporting plate material is aluminum, and the piezoelectric material is PZT2, as shown in Figure 28(b). Bandgaps are tuned based upon the optimization of the piezoelectric shunt impedance Z (iw). Two criteria were studied for the optimization; the first was to increase the metacomposites capability for decreasing the wave transmission capability, it was achieved by minimization of flexural wave energy velocities. The second criterion was to improve the wave's absorbing capacity of metacomposites; it was achieved by the computation of the dissipated electrical energy into the electrical shunt.

Ruzzene and Scarpa [125] studied the wave propagation characteristics in sandwich beams made up of periodic honeycombs acting as a cellular core. The sandwich beam model is used to predict the influence of cell periodicity on the beam and the impact of transverse vibration as well. Generally, core materials are placed periodically along the beam to introduce impedance mismatch that generates stopbands, and the wave cannot transmit through it. THE spectral FEM method was used here in place of the conventional FEM method to study the dynamic behavior of the structure. A theoretically developed model is used to obtain a transfer matrix to describe the wave propagation characteristics of a unit cell. This transfer matrix was then used to obtain dynamics stiffness matrix and formulate spectral finite element model.

Sandwich beam studied here whose core is composed of two different cellular solids arranged periodically alternatively along the beam length as shown in Figure 29. Hexagonal and auxetic honeycomb cores of various geometry shapes are used and analyzed. By varying the different elastic and mass properties of the two cores, impedance mismatch is generated that leads to the stopband patterns for a periodic structure. The sandwich beam transfer matrix is used to find the location of the stopband and study the influence of core geometry and periodicity on the stopbands through a series of simulations. It was concluded that the core geometries could be easily optimized to obtain stopband at desired frequency ranges, and the auxetic solids also provide great flexibility for the proper tuning of stop bands because of their curvature feature that helps in the manufacturing of curved shells. Therefore, the unique characteristics of cellular solids can be used to design light-weight composite beams for mechanical wave filtering.

Chen et al. [126] studied a class of architecture lattice metamaterials by replacing the regular straight beams with sinusoidal-shaped beams and evaluated their mechanical response and wave-propagation performance. This design was motivated by the concept that buckled structures have tunable phononic bandgap compared to conventional lattice metamaterials with small or no bandgaps. In addition to this, when buckled lattice metamaterials are subjected to uniaxial stretch, the local strain value is much smaller than the macroscopic strain; therefore, curved beams exhibit excellent stretchability under tension.

The proposed design was studied for different buckling modes, as shown in Figure 30. The design was subjected to large strains up-to 50% in tension for studying the auxetic

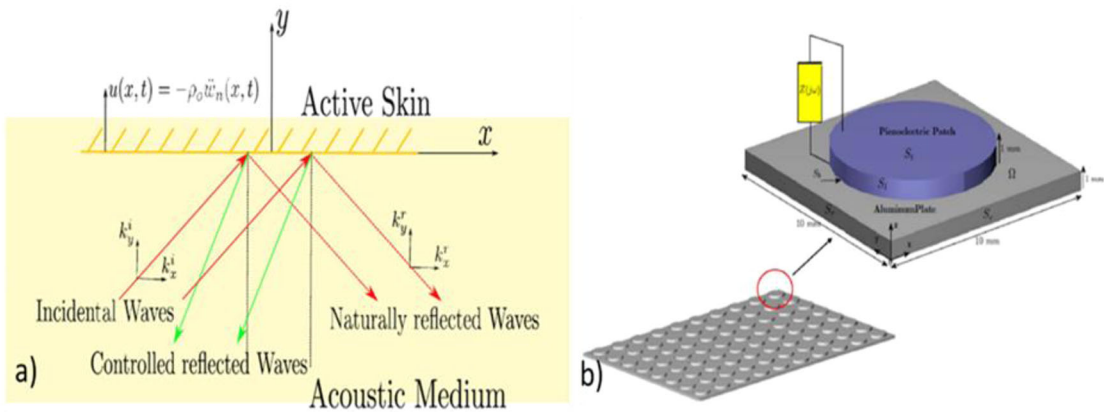


Figure 28. (a) Acoustic waves interacting with the active surface, (b) piezocomposite unit cell [48].

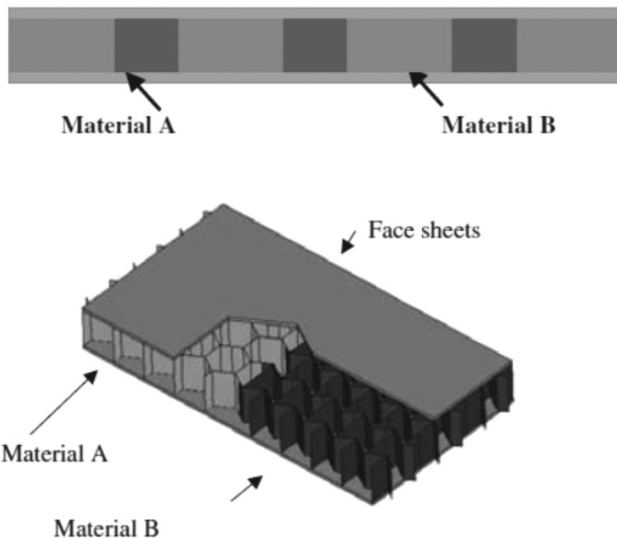


Figure 29. Sandwich beam with honeycomb core and unit cell [125].

response. The results indicated a large variation of Poisson's ratio between -0.7 and 0.5 ; it is attributed to the deformation pattern switching from bending dominated to stretching dominated within the curved beam. This transition phenomenon can be effectively controlled by tailoring the amplitude and wavelength of the sinusoidal beam. This interplay between the Poisson's ratio and the intrinsic architecture leads to exploring the behavior of metamaterial under elastic wave propagation. The dispersion analysis results in the formation of a complete bandgap due to local resonance and Bragg scattering phenomenon. This leads to further investigation for the dynamic tunability of the bandgap under the external mechanical stimulus, i.e., uniaxial tensile stretching. The results indicated that as the buckling modes increases, the bandgaps tends to shrink in with the increase of applied stretching. The deformation behavior along with the vibration-mitigation capability of the proposed lattice metamaterials makes it suitable to be used as programmable metamaterial for wave filtering and waveguiding.

Ouisse et al. [127] designed a new piezo-shunted kirigami auxetic lattice structure for wave filtering. The design consists of a pyramidal core with auxetic characteristics as the

base structure and shunted piezoelectric patches glued on it for controlling wave propagation. Architected materials such as kirigami cells modeled with smart systems improve the vibroacoustic property of structural components. The core of this design is modeled using the Japanese art technique of paper cutting/folding. The kirigami structure consists of a pyramidal shape unit cell that exhibits auxetic property ($-ve$ Poisson's ratio) and higher in-plane elastic properties than the out-of-plane ones.

The lattice is composed of periodic distribution of kirigami unit cells with shunted piezoelectric patches glued on each unit cell base, as shown in Figure 31. The combination of property induced by auxeticity and negative shunt circuit leads to the study of wave propagation characteristics. The controlling capability is obtained by correctly tuning the parameters of the external circuit to calculate effective total impedance for the desired frequency range. The particular bandwidth considered in this work is between 0 – 2.5 kHz, common for large scale airframe and transport structures. Various configurations were analyzed, such as the combination of short-circuit piezo-electric patches with negative impedance shunt and a resistance. It was concluded that the negative capacitance shunt cancels the bandgap at low frequency and results in a huge bandgap around 1100 to 2900 Hz. Adding resistance in the shunt circuit deteriorates negative capacitance performance by removing the bandgap in lower frequency ranges.

Ruzzene and Baz [106] studied the wave propagation in composite rods using Floquet's theorem and theory of periodic structures. Longitudinal wave propagation in the composite rod is controlled by using shape memory alloys (SMA) inserts arranged periodically along rods. The inserts provide the impedance mismatch with tunable characteristics to control the wave propagation. The study was performed in two steps. In the first step, one composite rod was made using two different materials arranged alternatively and periodically, as shown in Figure 32. The dispersion analysis was performed, and the bandgaps' width was studied for different frequency ranges and for varying geometrical and physical properties of the composites, i.e., the relative thickness of the layers and the relative impedance of the materials.

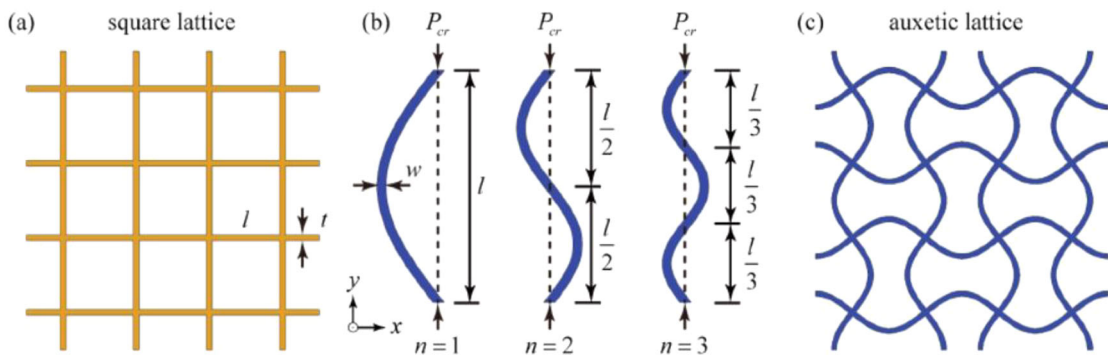


Figure 30. Schematic and deformation behavior of lattice material (a) square lattice with 2×2 unit cells, (b) buckling modes of a single sinusoidal beam under compression, (c) proposed architected lattice metamaterial with 2×2 unit cells [126].

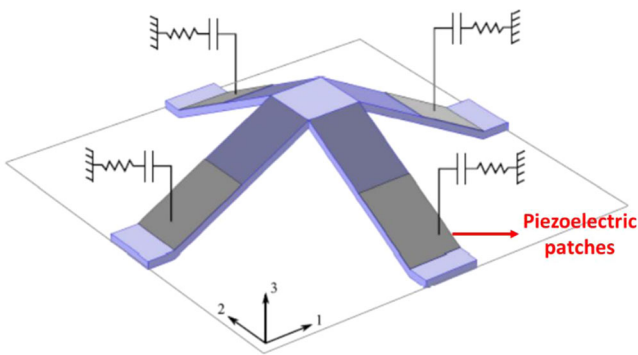


Figure 31. The piezocomposite periodic auxetic cell [127].

In the second step, the already developed concepts in the first step were used for designing the composite rods with SMA inserts. The shape memory alloy exhibits unique behavior that during thermal activation, Young's modulus of the inserts can vary up to three times as the alloy undergoes a phase transformation from martensite to austenite. The thermal activation of SMA can actively control the stopbands and width of the bandgap. The composite rod was analyzed for varying Elastic modulus and impedance values. The results indicated that wave attenuation capabilities increase for the relative impedance value smaller than 1, and the attenuation characteristics are also dependent on the relative thickness of layers that can be optimized based on the desired stopbands. This unique characteristic presents variable means for designing a variety of stable structures.

Airoldi and Ruzzene [49] studied the effect of employing periodic shunted piezoelectric patches for the designing of a tunable one-dimensional beam. This compact structure consists of a beam undergoing transverse and longitudinal motion bonded with a periodic array of piezoelectric patches with electrodes connected to a resonant electric circuit. This acousto-electrical system is characterized by the electrical resonances of the shunting circuits, and the resonant frequencies can be easily tuned by selecting the proper electrical impedance connected to each patch. This characterization leads to a new set of 1D metamaterials without the need for any structural modification.

The wave propagation characteristics were studied analytically through the Transfer Matrix approach and then validated by experimental means. The dispersion analysis

suggests the occurrence of stopband due to the internal resonance; the wave attenuation can be tuned by varying the frequency of the shunts. This behavior is achieved because of the coupling between the structural beam and the piezo patches, and it is found to be valid for both axial and bending wave motion. The analytical study suggests that this configuration behaves as a homogeneous structure with frequency-dependent and resonating mechanical properties.

Sugino et al. [128] analyzed wave attenuation through a fully programmable and digitally controlled metamaterial by the electromechanical implementation of an elastic waveguide. In this investigation, synthetic impedance circuits are used as active elements to digitally control the shunt circuit impedance for tuning resonant bandgap over a wide range of frequencies. A piezoelectric bimorph beam was considered, and piezo-ceramics were bonded to each pole in the thickness direction. The piezo-ceramic consists of a central shim, which is electrically grounded, and the opposite faces of each patch were bonded with thin metallic electrodes, as shown in Figure 33. The two opposing metallic electrodes were connected in parallel, and their resulting electrode pairs were shunted through a synthetic impedance circuit. The synthetic circuit used in this investigation was based on the Howland Current Pump (HCP), in which one of the terminals of the circuit is grounded; this makes the circuit to be used as an array of separate shunts on the same structure.

The experimental investigation exhibits a resonant bandgap that can be continuously shifted by digital tuning over a wide range of frequencies, i.e., 45 times the bandwidth of a fixed-frequency bandgap. The dynamic response of locally resonant metamaterial can be precisely controlled by externally programming the damping and bandwidth of the bandgap. The proposed active programmable configuration leads to a certain level of tunability that can be used to achieve a number of effective properties and characteristics.

Montgomery et al. [129] presented a new magneto-mechanical metamaterial that uses the bending mode technique obtained by coupling magnetic actuation and mechanical forces to achieve multi-physical property tunability. This new metamaterial employs asymmetric joint using hard magnetic soft active materials. Under the influence of the opposite direction, the magnetic field leads to a rapid

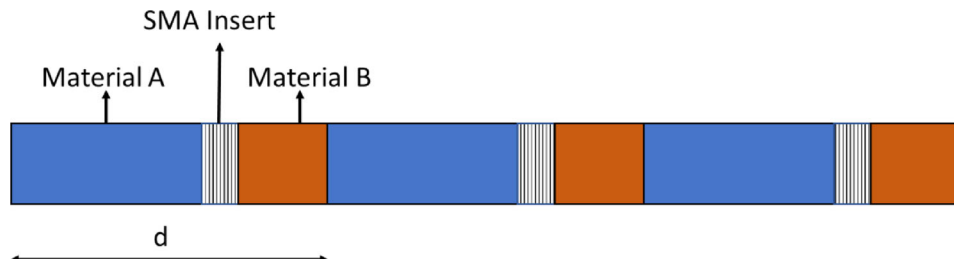


Figure 32. Schematic of periodic composite rod [106].

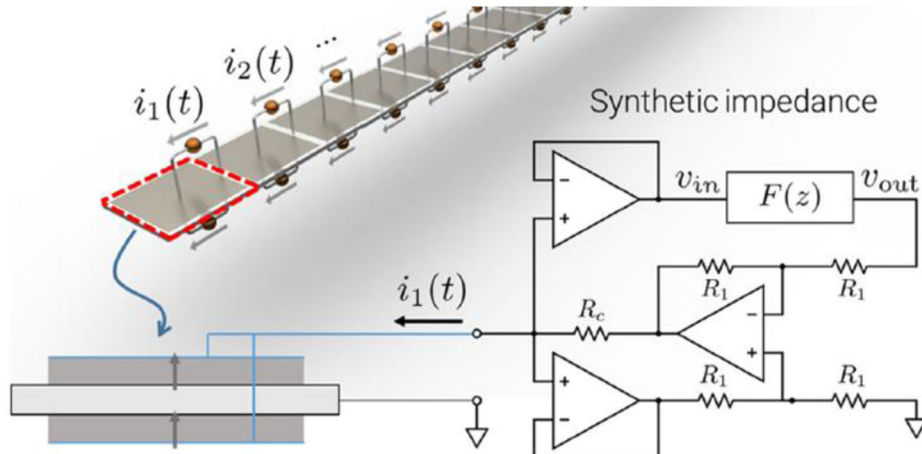


Figure 33. A schematic of the programmable piezoelectric locally resonant metamaterial. Thickness-poled piezoelectric patches are connected in parallel for bending vibration and shunted to synthetic impedance circuits [128].

transition between two actuation modes (folding and bending). The metamaterial suffers two distinct shapes under the subsequent application of compression force because of the deformation mode branching. One shape exhibits a topological transformation with a reduced number of pores in metastructures. This transformation empowers change in the physical behavior with a much broader range of tunability in properties such as bandgaps and mechanical stiffness. The other shape is unactuated metastructures having no bandgaps. Furthermore, this metamaterial design can also be incorporated with magnetic-shaped memory polymers to shift and tune the bandgap in unparalleled range due to stiffness tunability.

The effects of deformation mode branching on the bandgap of metamaterials under magneto-mechanical load are shown in Figure 34. Figure 34(a) shows the behavior of RVEs (Representative Volume Elements) along with the dispersion curves showing bandgap region under the influence of magnetic effect only. There is no noticeable bandgap in the undeformed material (at the center). As the magnetic field is applied, different bandgap emerges depending upon the direction of the magnetic field. Under the negative magnetic field, two bandgap emerges due to the folding deformation of the metastructures; there is a slight improvement in the bandwidth at high-frequency region as the magnetic field changes from -15mT to -30mT . In contrast, the bandwidth increases under the influence of positive magnetic field when it changes from $+7\text{mT}$ to $+20\text{mT}$; this happens because of the bending mode deformation.

Figure 34(b) and 34(c) shows the shift of bandgap when the mechanical force is applied along with the magnetic field. Figure 34(b) shows that under the compression strain of 10%, the bandwidth at high-frequency zone remains unchanged but moves slightly downwards. As the compression stress increases, the bandgap at the high-frequency range starts decreasing. Figure 34(c) shows that as the compressive strain increases, the bandgap at high-frequency region starts vanishing, and the bandgap at low-frequency region opens up. These results demonstrate the tunability enabled by the deformation mode under the magneto-mechanical load.

6. Conclusions and future research directions

The technical capability to manufacture the material in nanoscale led to the development of metamaterials. Metamaterials are artificially structured composites that are constructed using periodically arranged building blocks which not only enhance the properties of constituent materials but also give different functionalities and unusual properties like negative refractive index, negative mass density, negative Poisson's ratio, negative permittivity, negative permeability, negative modulus, sign reversal of thermal expansion coefficient and many more. These metamaterials are classified according to their effective parameters as electromagnetic metamaterial, optical metamaterial, acoustic metamaterial, and mechanical metamaterial. The mechanical metamaterials are classified based on elastic modulus, bulk and shear modulus, and Poisson's ratio. With the

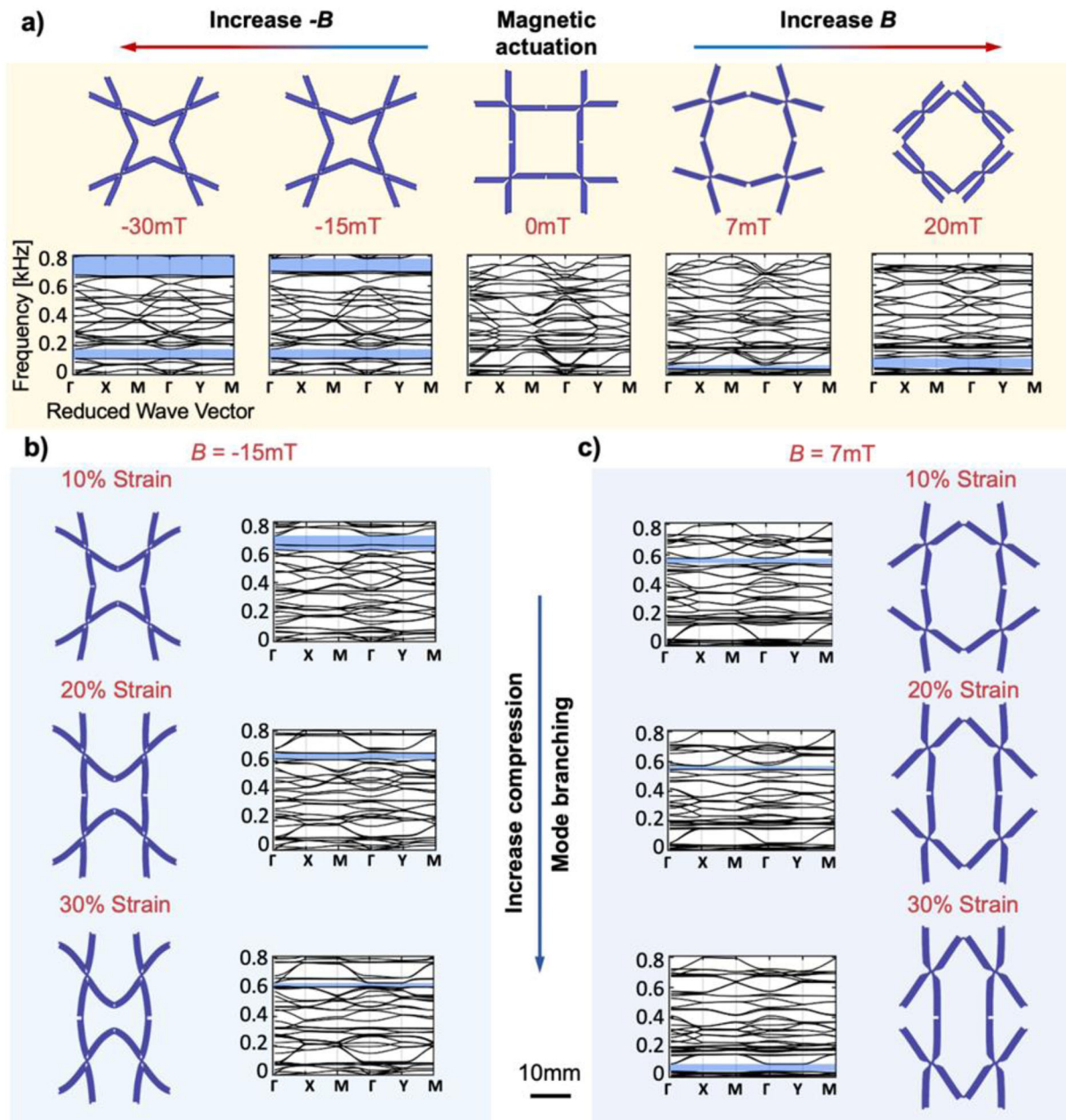


Figure 34. Effects of the deformation mode on metamaterials. (a) Behavior of RVEs and bandgap under magnetic field influence only, (b) behavior of RVEs and bandgap under influence of both compression load and negative magnetic field ($B = -15\text{mT}$), (c) behavior of RVEs and bandgap under influence of both compression load and positive magnetic field ($B = 7\text{mT}$) [129].

advancement in the fabrication techniques, sub-units have been constructed inside the building blocks of mechanical metamaterial, which under resonance condition couples with the propagating elastic waves to generate a wave attenuation region known as stopband; in mechanical terms, it is the zone where the vibration is isolated. The complex architecture of mechanical metamaterial used as sub-units arranged in an array result in the large bandgap, which means vibration isolation for a broad range of frequencies, this application of metamaterial has always been in high demand.

Two different mechanisms for vibration control are discussed, first by using passive mechanical metamaterial and the second by using it as an active one. The passive mechanism uses Bragg scattering and local resonance properties of the structure for the wave dispersion; different ways of

employing this concept are shown. The active one is based on the same concept as passive, with some external stimuli acting as an active element used for the further tuning of bandgaps without any change in the architecture of the proposed structure.

The advancement in the 3D printing techniques invented the Two-Photon Lithography technique, which manufactures mechanical metamaterial at the nanoscale, whereas Projection Micro Stereolithography techniques develop structure at the macro-scale. Recent developments have made the synthesis of ceramic or metallic mechanical metamaterial, which, after post-processing, gives properties like ultrahigh specific strength, ultra-lightweight, negative Poisson's ratio, high bulk to shear modulus ratio. These properties make a broad application of metamaterial in

different fields. Therefore, mechanical metamaterials are expected to begin a new era of materials.

The areas discussed in this review present a roadmap for the future directions of research on mechanical metamaterials. Many of the designs discussed in this review are studied theoretically and numerically. The advancement in 3D Printing technology will enable the theoretical concept to realize experimentally and study the mechanical behavior of metamaterials. Simultaneously, 3D Printing will also help to study fatigue behavior as the previous studies mostly focused on static, dynamic, and quasi-static behavior of mechanical metamaterials. Structural use of metamaterials for vibration control also requires a detailed study of fatigue behavior. For the active case, the multi-field coupling opens a new frontier for the development of a new class of metamaterial that can be used for wave attenuation without increasing the weight and size of the structure. These metamaterials can be used for energy harvesting purpose also.

Advancement in the design and simulation software will enable the generation of new design, modeling, and topological optimization by Artificial Intelligence (AI) techniques. AI has the ability to design geometrically optimized parts for the defined problem by basic parametric input (weight, strength, etc.). AI will play a big role in the industrial application of mechanical metamaterials, as AI reduces the cost to manufacture several samples for the testing, reduces time duration, and also helps in analyzing the characteristics and mechanical behavior of the metamaterials. AI technique will also be beneficial to study the functional property changes as the metamaterial is subjected to external vibration conditions. Mechanical metamaterials are expected to yield great breakthroughs in the future, depending on the foundation been laid.

Acknowledgments

The author would like to thank the Department of Mechanical Engineering and Industrial Design, National Institute of Technology Rourkela, for extending the facilities for this review.

Conflict of interest

The author declares that they have no known competing financial interests or personal relationships that could have appeared to influence the work reported in this paper

Funding

This research did not receive any specific grant from funding agencies in the public, commercial, or not-for-profit sectors.

ORCID

P. S. Balaji  <http://orcid.org/0000-0002-6364-4466>

References

- [1] N. Fleck, V. Deshpande, and M. Ashby, Micro-architected materials: Past, present and future, *Proc. R Soc. A*, vol. 466, no. 2121, pp. 2495–2516, 2010. DOI: [10.1098/rspa.2010.0215](https://doi.org/10.1098/rspa.2010.0215).
- [2] M. F. Ashby and D. R. H. Jones, *Engineering Materials 1: An Introduction to Properties, Applications and Design*, Vol. 1, Elsevier, Oxford, United Kingdom, 2012.
- [3] F. Libonati and M. J. Buehler, Advanced structural materials by bioinspiration, *Adv. Eng. Mater.*, vol. 19, no. 5, p. 1600787, 2017. DOI: [10.1002/adem.201600787](https://doi.org/10.1002/adem.201600787).
- [4] J. Bauer, et al., Approaching theoretical strength in glassy carbon nanolattices, *Nat. Mater.*, vol. 15, no. 4, pp. 438–443, 2016. DOI: [10.1038/nmat4561](https://doi.org/10.1038/nmat4561).
- [5] A. Vyatskikh, et al., Additive manufacturing of 3D nano-architected metals, *Nat. Commun.*, vol. 9, no. 1, pp. 593, 2018. DOI: [10.1038/s41467-018-03071-9](https://doi.org/10.1038/s41467-018-03071-9).
- [6] D. Jang and J. R. Greer, Transition from a strong-yet-brittle to a stronger-and-ductile state by size reduction of metallic glasses, *Nat. Mater.*, vol. 9, no. 3, pp. 215–219, 2010. DOI: [10.1038/nmat2622](https://doi.org/10.1038/nmat2622).
- [7] H. Gao, et al., Materials become insensitive to flaws at nanoscale: Lessons from nature, *Proc. Natl. Acad. Sci. USA*, vol. 100, no. 10, pp. 5597–5600, 2003. DOI: [10.1073/pnas.0631609100](https://doi.org/10.1073/pnas.0631609100).
- [8] J. H. Lee, J. P. Singer, and E. L. Thomas, Micro-/nanostructured mechanical metamaterials, *Adv. Mater.*, vol. 24, no. 36, pp. 4782–4810, 2012. DOI: [10.1002/adma.201201644](https://doi.org/10.1002/adma.201201644).
- [9] M. C. Moruzzi, M. Cinefra, and S. Bagassi, Vibroacoustic analysis of an innovative windowless cabin with metamaterial trim panels in regional turboprops, *Mech. Adv. Mater. Struct.*, vol. 26, pp. 1–13, 2019.
- [10] A. Srivastava, Elastic metamaterials and dynamic homogenization: A review, *Int. J. Smart Nano Mater.*, vol. 6, no. 1, pp. 41–60, 2015. DOI: [10.1080/19475411.2015.1017779](https://doi.org/10.1080/19475411.2015.1017779).
- [11] G. Singh and A. Marwaha, A review of metamaterials and its applications, *International Journal of Engineering Trends and Technology - IJETT*, vol. 19, pp. 305–310, 2015.
- [12] K. Kim and J. Ju, Mechanical metamaterials with 3D compliant porous structures, *Compos. Struct.*, vol. 132, pp. 874–884, 2015. DOI: [10.1016/j.compositesstructure.2015.06.060](https://doi.org/10.1016/j.compositesstructure.2015.06.060).
- [13] V. G. Veselago, The electrodynamics of substances with simultaneously negative values of ϵ and μ , *Sov. Phys. Usp.*, vol. 10, no. 4, pp. 509–514, 1968. DOI: [10.1070/PU1968v01n04ABEH003699](https://doi.org/10.1070/PU1968v01n04ABEH003699).
- [14] T. A. Schaedler, et al., Ultralight metallic microlattices, *Science*, vol. 334, no. 6058, pp. 962–965, 2011. DOI: [10.1126/science.1211649](https://doi.org/10.1126/science.1211649).
- [15] J. Li, et al., Experimental demonstration of an acoustic magnifying hyperlens, *Nat. Mater.*, vol. 8, no. 12, pp. 931–934, 2009. DOI: [10.1038/nmat2561](https://doi.org/10.1038/nmat2561).
- [16] Z. Liu, et al., Locally resonant sonic materials, *Science*, vol. 289, no. 5485, pp. 1734–1736, 2000. DOI: [10.1126/science.289.5485.1734](https://doi.org/10.1126/science.289.5485.1734).
- [17] Z. Yang, et al., Membrane-type acoustic metamaterial with negative dynamic mass, *Phys. Rev. Lett.*, vol. 101, no. 20, pp. 204301, 2008. DOI: [10.1103/PhysRevLett.101.204301](https://doi.org/10.1103/PhysRevLett.101.204301).
- [18] Z. Liu, C. T. Chan, and P. Sheng, Analytic model of phononic crystals with local resonances, *Phys. Rev. B*, vol. 71, no. 1, p. 014103, 2005. DOI: [10.1103/PhysRevB.71.014103](https://doi.org/10.1103/PhysRevB.71.014103).
- [19] N. S. Bakhvalov and G. Panasenko, *Homogenisation: Averaging Processes in Periodic Media: Mathematical Problems in the Mechanics of Composite Materials*, Vol. 36, Springer Science & Business Media, Dordrecht, The Netherlands, 2012.
- [20] V. V. Jikov, S. M. Kozlov, and O. A. Oleinik, *Homogenization of Differential Operators and Integral Functionals*, Springer Science & Business Media, Heidelberg, Germany, 2012.
- [21] C. M. Soukoulis and M. Wegener, Past achievements and future challenges in the development of three-dimensional photonic metamaterials, *Nature Photon.*, vol. 5, no. 9, pp. 523–530, 2011. DOI: [10.1038/nphoton.2011.154](https://doi.org/10.1038/nphoton.2011.154).
- [22] C. Kane and T. Lubensky, Topological boundary modes in isostatic lattices, *Nature Phys.*, vol. 10, no. 1, pp. 39–45, 2014. DOI: [10.1038/nphys2835](https://doi.org/10.1038/nphys2835).

- [23] X. Yu, et al., Mechanical metamaterials associated with stiffness, rigidity and compressibility: A brief review, *Prog. Mater. Sci.*, vol. 94, pp. 114–173, 2018. DOI: [10.1016/j.pmatsci.2017.12.003](https://doi.org/10.1016/j.pmatsci.2017.12.003).
- [24] X. Zhou, X. Liu, and G. Hu, Elastic metamaterials with local resonances: An overview, *Theor. Appl. Mech. Lett.*, vol. 2, no. 4, p. 041001, 2012. DOI: [10.1063/2.1204101](https://doi.org/10.1063/2.1204101).
- [25] L. Cvetcanin, M. Zukovic, and D. Cvetcanin, On the elastic metamaterial with negative effective mass, *J. Sound Vib.*, vol. 436, pp. 295–309, 2018. DOI: [10.1016/j.jsv.2018.06.066](https://doi.org/10.1016/j.jsv.2018.06.066).
- [26] N. Fang, et al., Ultrasonic metamaterials with negative modulus, *Nat. Mater.*, vol. 5, no. 6, pp. 452–456, 2006. DOI: [10.1038/nmat1644](https://doi.org/10.1038/nmat1644).
- [27] M. Kadic, et al., 3D metamaterials, *Nat. Rev. Phys.*, vol. 1, no. 3, pp. 198–210, 2019. DOI: [10.1038/s42254-018-0018-y](https://doi.org/10.1038/s42254-018-0018-y).
- [28] K. Bertoldi, et al., Flexible mechanical metamaterials, *Nat. Rev. Mater.*, vol. 2, no. 11, p. 17066, 2017. DOI: [10.1038/natrevmats.2017.66](https://doi.org/10.1038/natrevmats.2017.66).
- [29] S. Alexander, Amorphous solids: their structure, lattice dynamics and elasticity, *Phys. Rep.*, vol. 296, no. 2–4, pp. 65–236, 1998. DOI: [10.1016/S0370-1573\(97\)00069-0](https://doi.org/10.1016/S0370-1573(97)00069-0).
- [30] A. Rafsanjani, A. Akbarzadeh, and D. Pasini, Snapping mechanical metamaterials under tension, *Adv. Mater.*, vol. 27, no. 39, pp. 5931–5935, 2015. DOI: [10.1002/adma.201502809](https://doi.org/10.1002/adma.201502809).
- [31] R. L. Truby and J. A. Lewis, Printing soft matter in three dimensions, *Nature*, vol. 540, no. 7633, pp. 371–378, 2016.
- [32] D. J. Inman, *Vibration with Control*, John Wiley & Sons, West Sussex, 2017.
- [33] F. Fahy and J. Walker, *Advanced Applications in Acoustics, Noise and Vibration*, CRC Press, Trowbridge, Wiltshire, 2018.
- [34] D. P. Jena, S. N. Panigrahi, and R. Kumar, Gear fault identification and localization using analytic wavelet transform of vibration signal, *Measurement*, vol. 46, no. 3, pp. 1115–1124, 2013. DOI: [10.1016/j.measurement.2012.11.010](https://doi.org/10.1016/j.measurement.2012.11.010).
- [35] H. Boudaoud, et al., A shell finite element for active-passive vibration control of composite structures with piezoelectric and viscoelastic layers, *Mech. Adv. Mater. Struct.*, vol. 15, no. 3–4, pp. 208–219, 2008. DOI: [10.1080/15376490801907699](https://doi.org/10.1080/15376490801907699).
- [36] X. Wei, M. Zhu, and L. Jia, A semi-active control suspension system for railway vehicles with magnetorheological fluid dampers, *Veh. Syst. Dyn.*, vol. 54, no. 7, pp. 982–1003, 2016. DOI: [10.1080/00423114.2016.1177189](https://doi.org/10.1080/00423114.2016.1177189).
- [37] B. Mace, *Mechanical vibration: Analysis, uncertainties and control*—Third edition. HH Benaroya and ML Nagurka CRC Press, Taylor and Francis Group, 2 Park Square, Milton Park, Abingdon, Oxon, OX14 4RN, UK, 2010. 960pp. Illustrated.£44.99, *Aeronaut. J.*, vol. 115, no. 1172, pp. 650–650, 2011. ISBN 978-1-4200-8056-8. DOI: [10.1017/S000192400006345](https://doi.org/10.1017/S000192400006345).
- [38] J. S. Moita, et al., Analysis of active-passive plate structures using a simple and efficient finite element model, *Mech. Adv. Mater. Struct.*, vol. 18, no. 2, pp. 159–169, 2011. DOI: [10.1080/15376494.2010.496062](https://doi.org/10.1080/15376494.2010.496062).
- [39] P. S. Balaji and K. Karthik SelvaKumar, Applications of nonlinearity in passive vibration control: A review, *J. Vib. Eng. Technol.*, vol. 9, no. 2, pp. 183–213, 2021. DOI: [10.1007/s42417-020-00216-3](https://doi.org/10.1007/s42417-020-00216-3).
- [40] J. P. Amezquita-Sánchez, et al., Vibration control on smart civil structures: A review, *Mech. Adv. Mater. Struct.*, vol. 21, no. 1, pp. 23–38, 2014. DOI: [10.1080/15376494.2012.677103](https://doi.org/10.1080/15376494.2012.677103).
- [41] D. F. Ledezma-Ramírez, et al., Recent advances in shock vibration isolation: An overview and future possibilities, *Appl. Mech. Rev.*, vol. 71, no. 6, pp. 060802-1–060802-23, 2019. DOI: [10.1115/1.4044190](https://doi.org/10.1115/1.4044190).
- [42] Y. Wang, et al., Response and performance of a nonlinear vibration isolator with high-static-low-dynamic-stiffness under shock excitations, *J. Vibroeng.*, vol. 16, no. 7, pp. 3382–3398, 2014.
- [43] V. Smirnov and V. Mondrus, Comparison of linear and nonlinear vibration isolation system under random excitation, *Procedia Eng.*, vol. 153, pp. 673–678, 2016. DOI: [10.1016/j.proeng.2016.08.221](https://doi.org/10.1016/j.proeng.2016.08.221).
- [44] K. V. Eluri, et al., Analysis of Whole Body Vibration of a Two-Wheeler Rider, SAE International, Detroit, US, 2019.
- [45] W. Thomson, *Theory of Vibration with Applications*, CRC Press, London, England, 2018.
- [46] S. Yang, et al., Ultrasound tunneling through 3D phononic crystals, *Phys. Rev. Lett.*, vol. 88, no. 10, p. 104301, 2002. DOI: [10.1103/PhysRevLett.88.104301](https://doi.org/10.1103/PhysRevLett.88.104301).
- [47] M. Hirsekorn, et al., Modelling and simulation of acoustic wave propagation in locally resonant sonic materials, *Ultrasonics*, vol. 42, no. 1–9, pp. 231–235, 2004. DOI: [10.1016/j.ultras.2004.01.014](https://doi.org/10.1016/j.ultras.2004.01.014).
- [48] M. Collet, M. Ouisse, and F. Tateo, Adaptive metacomposites for vibroacoustic control applications, *IEEE Sens. J.*, vol. 14, no. 7, pp. 2145–2152, 2014. DOI: [10.1109/JSEN.2014.2300052](https://doi.org/10.1109/JSEN.2014.2300052).
- [49] L. Airolidi and M. Ruzzene, Design of tunable acoustic metamaterials through periodic arrays of resonant shunted piezos, *New J. Phys.*, vol. 13, no. 11, p. 113010, 2011. DOI: [10.1088/1367-2630/13/11/113010](https://doi.org/10.1088/1367-2630/13/11/113010).
- [50] W. Akl and A. Baz, Multi-cell active acoustic metamaterial with programmable bulk modulus, *J. Intell. Mater. Syst. Struct.*, vol. 21, no. 5, pp. 541–556, 2010. DOI: [10.1177/1045389X09359434](https://doi.org/10.1177/1045389X09359434).
- [51] M. A. Nouh, O. J. Aldraihem, and A. Baz, Periodic metamaterial plates with smart tunable local resonators, *J. Intell. Mater. Syst. Struct.*, vol. 27, no. 13, pp. 1829–1845, 2016. DOI: [10.1177/1045389X15615965](https://doi.org/10.1177/1045389X15615965).
- [52] H. Huang, C. Sun, and G. Huang, On the negative effective mass density in acoustic metamaterials, *Int. J. Eng. Sci.*, vol. 47, no. 4, pp. 610–617, 2009. DOI: [10.1016/j.ijengsci.2008.12.007](https://doi.org/10.1016/j.ijengsci.2008.12.007).
- [53] A. Søe-Knudsen, R. Darula, and S. Sorokin, Theoretical and experimental analysis of the stop-band behavior of elastic springs with periodically discontinuous of curvature, *J. Acoust. Soc. Am.*, vol. 132, no. 3, pp. 1378–1383, 2012. DOI: [10.1121/1.4740480](https://doi.org/10.1121/1.4740480).
- [54] J. Zhou, et al., Multi-low-frequency flexural wave attenuation in Euler-Bernoulli beams using local resonators containing negative-stiffness mechanisms, *Phys. Lett. A*, vol. 381, no. 37, pp. 3141–3148, 2017. DOI: [10.1016/j.physleta.2017.08.020](https://doi.org/10.1016/j.physleta.2017.08.020).
- [55] C. Sugino, et al., A general theory for bandgap estimation in locally resonant metastructures, *J. Sound Vib.*, vol. 406, pp. 104–123, 2017. DOI: [10.1016/j.jsv.2017.06.004](https://doi.org/10.1016/j.jsv.2017.06.004).
- [56] C. H. Park and A. Baz, Vibration control of beams with negative capacitive shunting of interdigital electrode piezoceramics, *J. Vib. Control*, vol. 11, no. 3, pp. 331–346, 2005. DOI: [10.1177/107754605040949](https://doi.org/10.1177/107754605040949).
- [57] N. W. Hagood and A. von Flotow, Damping of structural vibrations with piezoelectric materials and passive electrical networks, *J. Sound Vib.*, vol. 146, no. 2, pp. 243–268, 1991. DOI: [10.1016/0022-460X\(91\)90762-9](https://doi.org/10.1016/0022-460X(91)90762-9).
- [58] R. L. Forward, Electronic damping of vibrations in optical structures, *Appl. Opt.*, vol. 18, no. 5, pp. 690–697, 1979. DOI: [10.1364/AO.18.000690](https://doi.org/10.1364/AO.18.000690).
- [59] F.-L. Hsiao, et al., Waveguiding inside the complete band gap of a phononic crystal slab, *Phys. Rev. E Stat. Nonlin. Soft Matter Phys.*, vol. 76, no. 5 Pt 2, p. 056601, 2007. DOI: [10.1103/PhysRevE.76.056601](https://doi.org/10.1103/PhysRevE.76.056601).
- [60] T.-T. Wu, et al., Evidence of complete band gap and resonances in a plate with periodic stubbed surface, *Appl. Phys. Lett.*, vol. 93, no. 11, p. 111902, 2008. DOI: [10.1063/1.2970992](https://doi.org/10.1063/1.2970992).
- [61] R. Zhu, et al., Experimental and numerical study of guided wave propagation in a thin metamaterial plate, *Phys. Lett. A*, vol. 375, no. 30–31, pp. 2863–2867, 2011. DOI: [10.1016/j.physleta.2011.06.006](https://doi.org/10.1016/j.physleta.2011.06.006).
- [62] K. Lu, et al., Flexural vibration bandgaps of the multiple local resonance elastic metamaterial plates with irregular resonators, *Appl. Acoust.*, vol. 159, p. 107115, 2020. DOI: [10.1016/j.apacoust.2019.107115](https://doi.org/10.1016/j.apacoust.2019.107115).

- [63] J. Li, X. Fan, and F. Li, Numerical and experimental study of a sandwich-like metamaterial plate for vibration suppression, *Compos. Struct.*, vol. 238, p. 111969, 2020. DOI: [10.1016/j.compstruct.2020.111969](https://doi.org/10.1016/j.compstruct.2020.111969).
- [64] J.-H. He and H.-H. Huang, Complete vibrational bandgap in thin elastic metamaterial plates with periodically slot-embedded local resonators, *Arch. Appl. Mech.*, vol. 88, no. 8, pp. 1263–1274, 2018. DOI: [10.1007/s00419-018-1371-0](https://doi.org/10.1007/s00419-018-1371-0).
- [65] M. Reynolds and S. Daley, An active viscoelastic metamaterial for isolation applications, *Smart Mater. Struct.*, vol. 23, no. 4, p. 045030, 2014. DOI: [10.1088/0964-1726/23/4/045030](https://doi.org/10.1088/0964-1726/23/4/045030).
- [66] F. Aghighi, J. Morris, and A. V. Amirkhizi, Low-frequency micro-structured mechanical metamaterials, *Mech. Mater.*, vol. 130, pp. 65–75, 2019. DOI: [10.1016/j.mechmat.2018.12.008](https://doi.org/10.1016/j.mechmat.2018.12.008).
- [67] N. Kumar and S. Pal, Low frequency and wide band gap metamaterial with divergent shaped star units: Numerical and experimental investigations, *Appl. Phys. Lett.*, vol. 115, no. 25, p. 254101, 2019. DOI: [10.1063/1.5119754](https://doi.org/10.1063/1.5119754).
- [68] W. Elmadih, et al., Three-dimensional resonating metamaterials for low-frequency vibration attenuation, *Sci. Rep.*, vol. 9, no. 1, pp. 1–8, 2019. DOI: [10.1038/s41598-019-47644-0](https://doi.org/10.1038/s41598-019-47644-0).
- [69] L. D'Alessandro, et al., Low frequency 3D ultra-wide vibration attenuation via elastic metamaterial, *Sci. Rep.*, vol. 9, no. 1, pp. 1–8, 2019. DOI: [10.1038/s41598-019-44507-6](https://doi.org/10.1038/s41598-019-44507-6).
- [70] Y.-f Liu, et al., Trees as large-scale natural metamaterials for low-frequency vibration reduction, *Constr. Build. Mater.*, vol. 199, pp. 737–745, 2019. DOI: [10.1016/j.conbuildmat.2018.12.062](https://doi.org/10.1016/j.conbuildmat.2018.12.062).
- [71] A. Hussain and P. S. Balaji, Stiffness characteristics of a poly-cal wire rope isolators, *IOP Conf. Ser.: Mater. Sci. Eng.*, vol. 402, p. 012058, 2018. DOI: [10.1088/1757-899X/402/1/012058](https://doi.org/10.1088/1757-899X/402/1/012058).
- [72] R. Ibrahim, Recent advances in nonlinear passive vibration isolators, *J. Sound Vib.*, vol. 314, no. 3–5, pp. 371–452, 2008. DOI: [10.1016/j.jsv.2008.01.014](https://doi.org/10.1016/j.jsv.2008.01.014).
- [73] A. Carrella, et al., On the force transmissibility of a vibration isolator with quasi-zero-stiffness, *J. Sound Vib.*, vol. 322, no. 4–5, pp. 707–717, 2009. DOI: [10.1016/j.jsv.2008.11.034](https://doi.org/10.1016/j.jsv.2008.11.034).
- [74] J. Zhou, et al., Local resonator with high-static-low-dynamic stiffness for lowering band gaps of flexural wave in beams, *J. Appl. Phys.*, vol. 121, no. 4, p. 044902, 2017. DOI: [10.1063/1.4974299](https://doi.org/10.1063/1.4974299).
- [75] K. Wang, et al., Mathematical modeling and analysis of a meta-plate for very low-frequency band gap, *Appl. Math. Modell.*, vol. 73, pp. 581–597, 2019. DOI: [10.1016/j.apm.2019.04.033](https://doi.org/10.1016/j.apm.2019.04.033).
- [76] K. Wang, et al., Lower band gaps of longitudinal wave in a one-dimensional periodic rod by exploiting geometrical nonlinearity, *Mech. Syst. Sig. Process.*, vol. 124, pp. 664–678, 2019. DOI: [10.1016/j.ymssp.2019.02.008](https://doi.org/10.1016/j.ymssp.2019.02.008).
- [77] C. Cai, et al., Design and numerical validation of quasi-zero-stiffness metamaterials for very low-frequency band gaps, *Compos. Struct.*, vol. 236, p. 111862, 2020. DOI: [10.1016/j.compstruct.2020.111862](https://doi.org/10.1016/j.compstruct.2020.111862).
- [78] H. Fan, et al., Design of metastructures with quasi-zero dynamic stiffness for vibration isolation, *Compos. Struct.*, vol. 243, p. 112244, 2020. DOI: [10.1016/j.compstruct.2020.112244](https://doi.org/10.1016/j.compstruct.2020.112244).
- [79] K. Wang, et al., A semi-active metamaterial beam with electromagnetic quasi-zero-stiffness resonators for ultralow-frequency band gap tuning, *Int. J. Mech. Sci.*, vol. 176, p. 105548, 2020. DOI: [10.1016/j.ijmecsci.2020.105548](https://doi.org/10.1016/j.ijmecsci.2020.105548).
- [80] H. Sun, X. Du, and P. F. Pai, Theory of metamaterial beams for broadband vibration absorption, *J. Intell. Mater. Syst. Struct.*, vol. 21, no. 11, pp. 1085–1101, 2010. DOI: [10.1177/1045389X10375637](https://doi.org/10.1177/1045389X10375637).
- [81] G. W. Milton and J. R. Willis, On modifications of Newton's second law and linear continuum elastodynamics, *Proc. R Soc. A.*, vol. 463, no. 2079, pp. 855–880, 2007. DOI: [10.1098/rspa.2006.1795](https://doi.org/10.1098/rspa.2006.1795).
- [82] M. R. Haberman, et al., Negative stiffness metamaterials and periodic composites, *J. Acoust. Soc. Am.*, vol. 131, no. 4, pp. 3372–3372, 2012. DOI: [10.1121/1.4708717](https://doi.org/10.1121/1.4708717).
- [83] P. F. Pai, Metamaterial-based broadband elastic wave absorber, *J. Intell. Mater. Syst. Struct.*, vol. 21, no. 5, pp. 517–528, 2010. DOI: [10.1177/1045389X09359436](https://doi.org/10.1177/1045389X09359436).
- [84] H. Sun, X. Du, and P. F. Pai, Metamaterial broadband vibration absorbers by local resonance, 52nd AIAA/ASME/ASCE/AHS/ASC Structures, Structural Dynamics and Materials Conference 19th AIAA/ASME/AHS Adaptive Structures Conference 13t, 2011. DOI: [10.2514/6.2011-1781](https://doi.org/10.2514/6.2011-1781).
- [85] Z. Wu, et al., Band-gap property of a novel elastic metamaterial beam with X-shaped local resonators, *Mech. Syst. Sig. Process.*, vol. 134, p. 106357, 2019. DOI: [10.1016/j.ymssp.2019.106357](https://doi.org/10.1016/j.ymssp.2019.106357).
- [86] M. Nouh, O. Aldraihem, and A. Baz, Vibration characteristics of metamaterial beams with periodic local resonances, *J. Vib. Acoust.*, vol. 136, no. 6, pp. 061012-1–061012-12, 2014. DOI: [10.1115/1.4028453](https://doi.org/10.1115/1.4028453).
- [87] Y. Xiao, J. Wen, and X. Wen, Longitudinal wave band gaps in metamaterial-based elastic rods containing multi-degree-of-freedom resonators, *New J. Phys.*, vol. 14, no. 3, p. 033042, 2012. DOI: [10.1088/1367-2630/14/3/033042](https://doi.org/10.1088/1367-2630/14/3/033042).
- [88] X. Liu, et al., Wave propagation characterization and design of two-dimensional elastic chiral metacomposite, *J. Sound Vib.*, vol. 330, no. 11, pp. 2536–2553, 2011. DOI: [10.1016/j.jsv.2010.12.014](https://doi.org/10.1016/j.jsv.2010.12.014).
- [89] P. F. Pai, H. Peng, and S. Jiang, Acoustic metamaterial beams based on multi-frequency vibration absorbers, *Int. J. Mech. Sci.*, vol. 79, pp. 195–205, 2014. DOI: [10.1016/j.ijmecsci.2013.12.013](https://doi.org/10.1016/j.ijmecsci.2013.12.013).
- [90] A. Nanda and M. A. Karami, Tunable bandgaps in a deployable metamaterial, *J. Sound Vib.*, vol. 424, pp. 120–136, 2018. DOI: [10.1016/j.jsv.2018.03.015](https://doi.org/10.1016/j.jsv.2018.03.015).
- [91] C. Lv, et al., Origami based mechanical metamaterials, *Sci. Rep.*, vol. 4, p. 5979, 2014. DOI: [10.1038/srep05979](https://doi.org/10.1038/srep05979).
- [92] S. A. Zirbel, et al., Accommodating thickness in origami-based deployable arrays, *J. Mech. Des.*, vol. 135, no. 11, pp. 111005-1–111005-11, 2013. DOI: [10.1115/1.4025372](https://doi.org/10.1115/1.4025372).
- [93] J. P. Gardner, et al., The James Webb space telescope, *Space Sci. Rev.*, vol. 123, no. 4, pp. 485–606, 2006. DOI: [10.1007/s11214-006-8315-7](https://doi.org/10.1007/s11214-006-8315-7).
- [94] S. Felton, et al., Applied origami. A method for building self-folding machines, *Science*, vol. 345, no. 6197, pp. 644–646, 2014. DOI: [10.1126/science.1252610](https://doi.org/10.1126/science.1252610).
- [95] K. Kurabayashi, et al., Self-deployable origami stent grafts as a biomedical application of Ni-rich TiNi shape memory alloy foil, *Mater. Sci. Eng. A*, vol. 419, no. 1–2, pp. 131–137, 2006. DOI: [10.1016/j.msea.2005.12.016](https://doi.org/10.1016/j.msea.2005.12.016).
- [96] A. Spadoni, M. Ruzzene, and F. Scarpa, Dynamic response of chiral truss-core assemblies, *J. Intell. Mater. Syst. Struct.*, vol. 17, no. 11, pp. 941–952, 2006. DOI: [10.1177/1045389X06060219](https://doi.org/10.1177/1045389X06060219).
- [97] D. Beli, et al., Wave attenuation and trapping in 3D printed cantilever-in-mass metamaterials with spatially correlated variability, *Sci. Rep.*, vol. 9, no. 1, pp. 1–11, 2019. DOI: [10.1038/s41598-019-41999-0](https://doi.org/10.1038/s41598-019-41999-0).
- [98] H. Zhang, et al., Tunable acoustic filters assisted by coupling vibrations of a flexible Helmholtz resonator and a waveguide, *Appl. Phys. Lett.*, vol. 110, no. 17, p. 173506, 2017. DOI: [10.1063/1.4982635](https://doi.org/10.1063/1.4982635).
- [99] Y. Huang, et al., Pentamodal property and acoustic band gaps of pentamode metamaterials with different cross-section shapes, *Phys. Lett. A*, vol. 380, no. 13, pp. 1334–1338, 2016. DOI: [10.1016/j.physleta.2016.01.041](https://doi.org/10.1016/j.physleta.2016.01.041).
- [100] J. Wen, et al., Theoretical and experimental investigation of flexural wave propagation in straight beams with periodic structures: Application to a vibration isolation structure, *J. Appl. Phys.*, vol. 97, no. 11, p. 114907, 2005. DOI: [10.1063/1.1922068](https://doi.org/10.1063/1.1922068).

- [101] Z. Cheng, et al., Locally resonant periodic structures with low-frequency band gaps, *J. Appl. Phys.*, vol. 114, no. 3, p. 033532, 2013. DOI: [10.1063/1.4816052](https://doi.org/10.1063/1.4816052).
- [102] Y.-L. Tsai and T. Chen, Band gap structure of acoustic wave in hexagonal phononic crystals with polyethylene matrix, *Procedia Eng.*, vol. 79, pp. 612–616, 2014. DOI: [10.1016/j.proeng.2014.06.387](https://doi.org/10.1016/j.proeng.2014.06.387).
- [103] F. Javid, et al., Architected materials with ultra-low porosity for vibration control, *Adv. Mater.*, vol. 28, no. 28, pp. 5943–5948, 2016. DOI: [10.1002/adma.201600052](https://doi.org/10.1002/adma.201600052).
- [104] X. Ding, et al., Controllable propagation of bending waves in wrinkled films, *J. Appl. Mech.*, vol. 86, no. 6, pp. 061005-1–061005-8, 2019. DOI: [10.1115/1.4043073](https://doi.org/10.1115/1.4043073).
- [105] K. Bertoldi and M. C. Boyce, Wave propagation and instabilities in monolithic and periodically structured elastomeric materials undergoing large deformations, *Phys. Rev. B*, vol. 78, no. 18, p. 184107, 2008. DOI: [10.1103/PhysRevB.78.184107](https://doi.org/10.1103/PhysRevB.78.184107).
- [106] M. Ruzzene and A. Baz, Control of wave propagation in periodic composite rods using shape memory inserts, *J. Vib. Acoust.*, vol. 122, no. 2, pp. 151–159, 2000. DOI: [10.1115/1.568452](https://doi.org/10.1115/1.568452).
- [107] M. Ruzzene and A. Baz, Attenuation and localization of wave propagation in periodic rods using shape memory inserts, *Smart Mater. Struct.*, vol. 9, no. 6, pp. 805–816, 2000. DOI: [10.1088/0964-1726/9/6/310](https://doi.org/10.1088/0964-1726/9/6/310).
- [108] A. Baz, Active control of periodic structures, *J. Vib. Acoust.*, vol. 123, no. 4, pp. 472–479, 2001. DOI: [10.1115/1.1399052](https://doi.org/10.1115/1.1399052).
- [109] A. Bergamini, et al., Phononic crystal with adaptive connectivity, *Adv. Mater.*, vol. 26, no. 9, pp. 1343–1347, 2014. DOI: [10.1002/adma.201305280](https://doi.org/10.1002/adma.201305280).
- [110] F. Casadei, et al., Vibration control of plates through hybrid configurations of periodic piezoelectric shunts, *J. Intell. Mater. Syst. Struct.*, vol. 23, no. 10, pp. 1169–1177, 2012. DOI: [10.1177/1045389X124443014](https://doi.org/10.1177/1045389X124443014).
- [111] M. Collet, et al., Semi-active optimization of 2D wave dispersion into shunted piezo-composite systems for controlling acoustic interaction, *Smart Mater. Struct.*, vol. 21, no. 9, p. 094002, 2012. DOI: [10.1088/0964-1726/21/9/094002](https://doi.org/10.1088/0964-1726/21/9/094002).
- [112] S. Chen, et al., Wave propagation and attenuation in plates with periodic arrays of shunted piezo-patches, *J. Sound Vib.*, vol. 332, no. 6, pp. 1520–1532, 2013. DOI: [10.1016/j.jsv.2012.11.005](https://doi.org/10.1016/j.jsv.2012.11.005).
- [113] P. Celli and S. Gonella, Tunable directivity in metamaterials with reconfigurable cell symmetry, *Appl. Phys. Lett.*, vol. 106, no. 9, p. 091905, 2015. DOI: [10.1063/1.4914011](https://doi.org/10.1063/1.4914011).
- [114] J. Wen, et al., Directionality of wave propagation and attenuation in plates with resonant shunting arrays, *J. Intell. Mater. Syst. Struct.*, vol. 27, no. 1, pp. 28–38, 2016. DOI: [10.1177/1045389X14560361](https://doi.org/10.1177/1045389X14560361).
- [115] F. Tateo, et al., Experimental characterization of a bi-dimensional array of negative capacitance piezo-patches for vibroacoustic control, *J. Intell. Mater. Syst. Struct.*, vol. 26, no. 8, pp. 952–964, 2015. DOI: [10.1177/1045389X14536006](https://doi.org/10.1177/1045389X14536006).
- [116] R. Zhu, et al., Experimental study of an adaptive elastic metamaterial controlled by electric circuits, *Appl. Phys. Lett.*, vol. 108, no. 1, p. 011905, 2016. DOI: [10.1063/1.4939546](https://doi.org/10.1063/1.4939546).
- [117] H. Zhang, et al., Soft mechanical metamaterials with unusual swelling behavior and tunable stress-strain curves, *Sci. Adv.*, vol. 4, no. 6, p. eaar8535, 2018. DOI: [10.1126/sciadv.aar8535](https://doi.org/10.1126/sciadv.aar8535).
- [118] P. Pitchappa, et al., Microelectromechanically reconfigurable interpixelated metamaterial for independent tuning of multiple resonances at terahertz spectral region, *Optica*, vol. 2, no. 6, pp. 571–578, 2015. DOI: [10.1364/OPTICA.2.000571](https://doi.org/10.1364/OPTICA.2.000571).
- [119] M. Bodaghi and W. Liao, 4D printed tunable mechanical metamaterials with shape memory operations, *Smart Mater. Struct.*, vol. 28, no. 4, p. 045019, 2019. DOI: [10.1088/1361-665X/ab0b6b](https://doi.org/10.1088/1361-665X/ab0b6b).
- [120] S. Wu, et al., Symmetry-breaking actuation mechanism for soft robotics and active metamaterials, *ACS Appl. Mater. Interfaces*, vol. 11, no. 44, pp. 41649–41658, 2019. DOI: [10.1021/acsami.9b13840](https://doi.org/10.1021/acsami.9b13840).
- [121] M. Lei, et al., Magnetically tunable metamaterial perfect absorber, *J. Appl. Phys.*, vol. 119, no. 24, p. 244504, 2016. DOI: [10.1063/1.4954224](https://doi.org/10.1063/1.4954224).
- [122] C. Yang, et al., 4D printing reconfigurable, deployable and mechanically tunable metamaterials, *Mater. Horiz.*, vol. 6, no. 6, pp. 1244–1250, 2019. DOI: [10.1039/C9MH00302A](https://doi.org/10.1039/C9MH00302A).
- [123] K. Yi, et al., Active metamaterials with broadband controllable stiffness for tunable band gaps and non-reciprocal wave propagation, *Smart Mater. Struct.*, vol. 28, no. 6, p. 065025, 2019. DOI: [10.1088/1361-665X/ab19dc](https://doi.org/10.1088/1361-665X/ab19dc).
- [124] T. Ren, et al., Active tunability of band gaps for a novel elastic metamaterial plate, *Acta Mech.*, vol. 231, no. 10, pp. 4035–4053, 2020. DOI: [10.1007/s00707-020-02728-1](https://doi.org/10.1007/s00707-020-02728-1).
- [125] M. Ruzzene and F. Scarpa, Control of wave propagation in sandwich beams with auxetic core, *J. Intell. Mater. Syst. Struct.*, vol. 14, no. 7, pp. 443–453, 2003. DOI: [10.1177/1045389X03035515](https://doi.org/10.1177/1045389X03035515).
- [126] Y. Chen, et al., Lattice metamaterials with mechanically tunable Poisson's ratio for vibration control, *Phys. Rev. Appl.*, vol. 7, no. 2, p. 024012, 2017. DOI: [10.1103/PhysRevApplied.7.024012](https://doi.org/10.1103/PhysRevApplied.7.024012).
- [127] M. Ouisse, M. Collet, and F. Scarpa, A piezo-shunted kirigami auxetic lattice for adaptive elastic wave filtering, *Smart Mater. Struct.*, vol. 25, no. 11, p. 115016, 2016. DOI: [10.1088/0964-1726/25/11/115016](https://doi.org/10.1088/0964-1726/25/11/115016).
- [128] C. Sugino, M. Ruzzene, and A. Erturk, Digitally programmable resonant elastic metamaterials, *Phys. Rev. Appl.*, vol. 13, no. 6, p. 061001, 2020. DOI: [10.1103/PhysRevApplied.13.061001](https://doi.org/10.1103/PhysRevApplied.13.061001).
- [129] S. M. Montgomery, et al., Magneto-mechanical metamaterials with widely tunable mechanical properties and acoustic band-gaps, *Adv. Funct. Mater.*, vol. 31, no. 3, p. 2005319, 2021. DOI: [10.1002/adfm.202005319](https://doi.org/10.1002/adfm.202005319).